

Passive Control of Bridge Wind-Induced Instabilities by Tuned Mass Dampers and Movable Flaps

K.N. Bakis¹, M. Massaro², M.S. Williams³, and J.M.R. Graham⁴

¹Department of Engineering Science, University of Oxford, Parks Road, Oxford OX1 3PJ, U.K..

Email: konstantinos-nikolaos.bakis@eng.ox.ac.uk

²Department of Industrial Engineering, University of Padova, Via Venezia 1, 35131 Padova, Italy

³Department of Engineering Science, University of Oxford, Parks Road, Oxford OX1 3PJ, U.K.

⁴Department of Aeronautics, Imperial College London, London SW7 2AZ, UK

ABSTRACT

This study investigates different ways to passively suppress wind-induced instabilities such as flutter and torsional divergence. The control system design study is based on a sectional flexible bridge model interacting with a constant velocity airstream. Two different strategies are considered, separately and in combination. The first makes use of trailing and leading flaps adjacent to the bridge deck, the motion of which is triggered by the deck's movement through a combination of springs, dampers and inerters at the hinged connection. Emphasis is placed on the effect of the flap hinge location and an optimization procedure is used for determining the compensator parameters that result in favorable aeroelastic properties. The second approach reexamines the efficacy and limitations of using Tuned Mass Dampers (TMDs) placed inside the bridge deck for controlling self-excited motion. We conclude by combining the two approaches and introducing a kinematic constraint between the masses of the TMD and the flaps. This combined mechanical system, referred to as the Flap Mass Damper (FMD), combines favorable aerodynamic properties of the flaps with a driving force provided by the vibrating mass. Consequently it has the advantage of not requiring complex and often impractical linkages in order to transmit the deck motion to the flaps.

Special attention is given to ensuring that the passive control system attains optimum robustness properties and maximizes tolerance to uncertainties. Uncertainties are quantified in a series of simulations showing how the alteration of the bridge's natural frequencies affect the stability of the controlled system. The Humber Bridge in the U.K. is chosen as an example for the numerical simulations.

INTRODUCTION

No problem in the field of civil-engineering-related aeroelastic instabilities has received the publicity afforded the collapse of the Tacoma Narrows Bridge in November 1940. This disaster triggered the development of modern bridge aeroelasticity and marked the beginning of quantitative study in bridge aerodynamics. The mathematical framework for treating the thin plate flutter instability problem is attributed to (Theodorsen 1934). Later (Scanlan and Tomko 1971) introduced the use of reduced-frequency dependent functions, commonly known as flutter derivatives, in an attempt to take into account the deck's bluffness. This is of particular importance for deep truss decked girders, which bear little resemblance to thin plate plate aerodynamics. Flutter (Hodges and Pierce 2002; Billah and Scanlan 1991; Scanlan 1978) is an aeroelastic instability that can occur in steady wind conditions, of sufficiently high speed, and results from small movements of the structure producing changes in the aerodynamic forces being exerted on the structure, and vice versa. These bi-directional interactions between the flexible structure and the air stream set up a feedback loop, which becomes unstable due to negative damping at high wind speeds. One or more structural modes can participate in flutter, and the resulting instability will eventually lead to structural failure.

Increasing span lengths pose a challenge to aeroelastic stability and experience gained from record span projects such as the Akashi Kaikyo Bridge and Great Belt East Bridge has shown that classic aerodynamic design either in the form of deep truss girders (Akashi Bridge) or the more modern flat box girder solution (Humber, Bosphorus, Great Belt) reaches its limit for spans approaching 2000m (Diana et al. 1998). Countermeasures to overcome this limitation can be classified in three categories. The first approach consists in reducing aerodynamic forces by altering

the shape of the deck section. For example, the proposed triple-girder deck solution, having total deck width of 60m, for the 3.3km long Messina Strait Bridge results in an estimation of flutter wind speed of 80m/s (Xiang and Ge 2003). Furthermore, Larsen's analytical investigations and wind tunnel studies have shown that slotting the deck is an effective approach for improving aerodynamic performance (Larsen et al. 1998). Vertical and horizontal stabilizers (Makoto 2004) as well as fixed winglets fall into the same category. These methods have the advantage of providing a passive static solution to the problem. However, as span lengths increase, the economical efficiency of these methods declines due to the necessary increase in girder separation. There are also construction and maintenance issues which need to be addressed (Li et al. 2015). The second approach introduces structural modifications usually related to the cable system for increased torsional stiffness (Gimsing 1997). This approach has some advantages in terms of increased flutter stability boundaries, but demands far more complicated construction process and material quantity.

The work at hand is focused on the third alternative; which relies on actively or passively controlled devices for generating stabilizing forces against aerodynamic loading. Perhaps the most effective physical control measures is the introduction of auxiliary flaps either adjacent to the deck or at some distance above or below it, Fig. 1. The first configuration accounts for the aerodynamic interference between the deck and the flaps whereas the second considers the deck and flaps to be independent surfaces. The control of bridge flutter using actively controlled flaps located beneath the deck was first proposed in (Ostenfeld and Larsen 1992) and further investigation was later undertaken in (Hansen and Thoft-Christensen 2001). More recently (Li et al. 2015) based on a two dimensional active control framework, performed an active control procedure using a pair of rotatable winglets at a distance from the deck. Ref. (Boberg et al. 2015) performed an experimental investigation employing controllable arrays of flaps using simple and manually tuned control algorithms based on pure gain and phase-shifting for the flap actuation. Optimal control strategies of this sort as well as pole placement algorithms provide a computationally viable procedure for deriving stabilizing controllers but neglect robustness properties and the assessment of available stability margins with respect to plant uncertainties. Indeed, for a controllable and

observable system the computation of a stabilizing controller is a straight forward design exercise but investigation by the authors has shown that it can lead to very poor robustness margins. To address this issue (Bakis et al. 2016) developed a framework for investigating flap efficiency on a full bridge multi-modal model while implementing an H_∞ active control strategy for quantifying structural and aerodynamic uncertainty. It was shown that, although the system can be stabilized fairly easily, the controlled system loses robustness rapidly for wind-speeds above the uncontrolled torsional divergence speed. The optimum flap length configuration has been determined for a full bridge case.

Contrary to active systems, passive flap mechanisms have the advantage of dispensing the need for an external power source, but require an elaborate mechanical network for transforming deck movement into flap rotation. Ideally, a feedback connection between deck rotational movement, rotation being the dominant mode in flutter coupling, and the flap rotations should be established. The main practical implication of this endeavour arises due to lack of access to a ground reference frame. Ref. (Omenzetter et al. 2000a; Omenzetter et al. 2000b) proposed a mechanical system in which the flap rotation is linked to the deck pitch motion by means of additional cables and an auxiliary transverse beam supported by the main cables Fig. 2 (a). Prestressed springs are used to push the flaps since the cables only provide tensile forces. Sectional analysis of this system showed that although higher critical wind speed can be attained, large flaps are required as well as significant stiffness for the supporting beam. A subsequent finite element aeroelastic framework showed that due to kinematic coupling between the flap rotation and the sway motion of the deck and cables, the achievable improvement in the bridge's critical flutter speed is limited (Omenzetter et al. 2002a; Omenzetter et al. 2002b). Ref. (Wilde et al. 1999) proposed an alternative mechanism in which the flaps are kinematically constrained by a pendulum inside the deck, Fig. 2 b). More recently (Phan and Nguyen 2013) proposed a mechanism based on a cross beam, surrounding the deck girder, attached to the hanger cables with additional gears and a belt for driving flap motion. The system results in a pure gain control law. The cross beam is used as a reference for pitch rotation, but hinders the mechanism's applicability on real structures due to its construction

complexity and aerodynamic modification of the deck girder.

Pure gain controllers like these however forego the advantages that accrue from phase compensation, whereas fixed-phase controllers are not physically realizable. Ref. (Xiaowei et al. 2014) introduced phase compensation and used an optimization routine for determining the controllers parameters. However the proposed design was only realizable under the premise that it can be connected to an inertial reference frame, which is very difficult in practice. The feasibility of passive control of schemes on the erection stage of suspension bridges for flutter and buffeting has been investigated in (Bakis et al. 2015; Massaro et al. 2015) and some efforts have been made to combine the advantages of control surfaces with a Tuned Mass Damper (TMD) (Kwon et al. 2000; Starossek and Aslan 2008) although a detailed analysis has not been reported yet. Up to date there has been no practical application of implementing actively or passively controlled flaps to a bridge, because their reliability and effectiveness has not been clearly demonstrated. Control of flutter and buffeting of suspension bridges has also been addressed using single Tuned Mass Dampers TMDs (Fujino and Abe 1993; Chen and Kareem 2000; Lin et al. 2003) or Multiple TMDs (MTMDs) (Kwon and Park 2004; Pourzeynali and Datta 2005). The tuning parameters are usually based on simplified design formulas (Den Hartog 1985; Fujino and Abe 1993) to tune the TMD degrees of freedom close to the frequencies corresponding to vertical and torsional symmetric modes of the bridge, which couple during flutter. However, the performance of a TMD is significantly degraded by off-tuning or off-optimum damping in the TMD (Kwon and Park 2004). The MTMD, consisting of a large number of small TMDs, can cover a frequency band around the modes to be controlled. However, this approach significantly increases the complexity and applicability of the solution. Other types of passive control have also been used to improve aerodynamic stability, for example placing tanks of water on deck, or using an eccentric mass on the windward side.

The novelty of this work consists in devising a passively controlled deck-flap network without the need of external impractical linkages. We also pay special attention to robustness against uncertainties, a fundamental issue often evaded in previous studies. First, a kinematic flap arrangement is introduced, which is based on a general passive controller, including inerters, rather than the

classical spring-damper configuration. An important advantage is that there is no need for pre-selecting the network layout, which is instead determined by an optimization process. Second, we make use of suspended masses inside the box girder to provide a driving force to the flaps through a simple linkage. The proposed mechanical layout avoids the use of external components, which interfere with the deck's aerodynamic characteristics, and of additional cables which complicate the system and increase dead load.

DYNAMIC MODEL OF THE DECK-FLAP PASSIVE SYSTEM

In this section a controllable leading-and trailing-edge flap is used to suppress aeroelastic instabilities; the flap torques are the controllable inputs. The components of the system model are described in the following sections.

Structural Model

The kinematic model of the deck-flap system is assumed to have four degrees of freedom $q = \{h, \alpha, \beta_l, \beta_t\}^T$, Fig. 3. These are the deck's pitch angle α , and heave h with respect to the elastic centre and the leading-and trailing-edge relative to the deck flap angles β_l and β_t respectively. Sway motion of the deck and main cables as well as changes in the hanger length are neglected.

The equations of motion can be derived using the Lagrange's approach

$$\frac{d}{dt} \left(\frac{\partial L}{\partial \dot{q}_i} \right) - \frac{\partial L}{\partial q_i} + \frac{\partial D}{\partial \dot{q}_i} = Q_i \quad (i = 1..4) \quad (1)$$

where $L = T - V$ with T the kinetic energy and V the potential energy, D is the dissipation function and Q_i the generalized force associated with q_i . The kinetic energy of the deck T_d , leading flap T_l and trailing flap T_t can be computed by integration over the deck and flap domains A_d , A_l and A_t :

$$T_d = \frac{1}{2} \int_{A_d} (\dot{h} + r\dot{\alpha})^2 dm \quad T_l = \frac{1}{2} \int_{A_l} (\dot{h} + r\dot{\alpha} - \dot{\beta}_l (r - r_{\beta_l}))^2 dm \quad T_t = \frac{1}{2} \int_{A_t} (\dot{h} + r\dot{\alpha} + \dot{\beta}_t (r - r_{\beta_t}))^2 dm. \quad (2)$$

The potential energy V and dissipation function D associated to the springs and dampers read:

$$V = \frac{1}{2} (K_h h^2 + K_\alpha \alpha^2 + K_{\beta_l} \beta_l^2 + K_{\beta_t} \beta_t^2), \quad D = \frac{1}{2} (C_h \dot{h}^2 + C_\alpha \dot{\alpha}^2 + C_{\beta_l} \dot{\beta}_l^2 + C_{\beta_t} \dot{\beta}_t^2). \quad (3)$$

The generalized forces can be computed from the virtual work δW

$$\delta W = L\delta h + M\delta\alpha + (M^{\beta_l} + M_c^{\beta_l})\delta\beta_l + (M^{\beta_t} + M_c^{\beta_t})\delta\beta_t \rightarrow Q = \{L, M, M^{\beta_l} + M_c^{\beta_l}, M^{\beta_t} + M_c^{\beta_t}\}^T \quad (4)$$

The resulting equations of motion are

$$\text{Deck-lift : } m\ddot{h} + S_\alpha \ddot{\alpha} + S_{\beta_l} \ddot{\beta}_l + S_{\beta_t} \ddot{\beta}_t + C_h \dot{h} + K_h h = L, \quad (5)$$

$$\text{Deck-moment : } S_\alpha \ddot{h} + I_\alpha \ddot{\alpha} - (I_{\beta_l} - r_{\beta_l} S_{\beta_l}) \ddot{\beta}_l + (I_{\beta_t} + r_{\beta_t} S_{\beta_t}) \ddot{\beta}_t + C_\alpha \dot{\alpha} + K_\alpha \alpha = M, \quad (6)$$

$$\text{Leading-flap moment : } S_{\beta_l} \ddot{h} - (I_{\beta_l} - r_{\beta_l} S_{\beta_l}) \ddot{\alpha} + I_{\beta_l} \ddot{\beta}_l + C_{\beta_l} \dot{\beta}_l + K_{\beta_l} \beta_l = M^{\beta_l} + M_c^{\beta_l}, \quad (7)$$

$$\text{Trailing-flap moment : } S_{\beta_t} \ddot{h} + (I_{\beta_t} + r_{\beta_t} S_{\beta_t}) \ddot{\alpha} + I_{\beta_t} \ddot{\beta}_t + C_{\beta_t} \dot{\beta}_t + K_{\beta_t} \beta_t = M^{\beta_t} + M_c^{\beta_t}, \quad (8)$$

where m is the mass per unit length of the deck-flaps combination, while S_α , S_{β_l} and S_{β_t} are given by (see Fig. 3 b):

$$S_\alpha = \int_{A_d + A_l + A_t} r dm \quad S_{\beta_l} = - \int_{A_l} (r - r_{\beta_l}) dm \quad \text{and} \quad S_{\beta_t} = \int_{A_t} (r - r_{\beta_t}) dm. \quad (9)$$

The per-unit-length moments of inertia I_α , I_{β_l} and I_{β_t} are given by:

$$I_\alpha = \int_{A_d + A_l + A_t} r^2 dm \quad I_{\beta_l} = \int_{A_l} (r - r_{\beta_l})^2 dm \quad \text{and} \quad I_{\beta_t} = \int_{A_t} (r - r_{\beta_t})^2 dm \quad (10)$$

The quantities m_d , m_{β_l} and m_{β_t} are the masses per unit span length of the deck and leading-trailing flaps respectively (note: $m = m_d + m_{\beta_l} + m_{\beta_t}$). I_α , I_{β_l} and I_{β_t} are the (per unit length) mass moments of inertia of the deck with respect to the elastic center and mass moment of inertia of the flaps with respect to the deck-flaps hinges. K_h and K_α are the per unit length vertical and torsional

stiffness of the entire assembly; K_{β_l} and K_{β_t} are the per unit length leading-and trailing- edge torsional stiffnesses of the flaps with respect to the hinges. For a given bridge the heave and torsion resonant frequencies ω_h and ω_α are assumed known, The corresponding stiffnesses are computed as $K_h = m\omega_h^2$ and $K_\alpha = I_\alpha\omega_\alpha^2$. The flap frequencies ω_{β_l} and ω_{β_t} are similarly computed by $K_{\beta_l} = I_{\beta_l}\omega_{\beta_l}^2$ and $K_{\beta_t} = I_{\beta_t}\omega_{\beta_t}^2$. Similarly, the damping terms are: $C_h = 2\zeta_h\omega_h m$, $C_\alpha = 2\zeta_\alpha\omega_\alpha I_\alpha$, $C_{\beta_l} = 2\zeta_{\beta_l}\omega_{\beta_l} I_{\beta_l}$ and $C_{\beta_t} = 2\zeta_{\beta_t}\omega_{\beta_t} I_{\beta_t}$, where ζ_{β_l} , ζ_{β_t} are the corresponding damping ratios. L and M are the aerodynamic lift and moment on the bridge deck. The aerodynamic moments M^{β_l} and M^{β_t} act respectively around the leading and trailing flap hinges. $M_c^{\beta_l}$ and $M_c^{\beta_t}$ are the input control torques to the system.

The flaps can be thought as an internal part of the deck or as an extension to the existing bridge girder. In the first case the deck half chord b is kept the same, whereas in the second case it needs to be updated in order to include the additional flap width. Further details on the aerodynamic flap shape is given in (Gouder et al. 2015). In this study we make use of the Humber Bridge as an example for simulations. The parameter values used are given in Table 1, in which ρ_f and d_f are the flap mass density and thickness respectively. The mass of the leading and trailing flaps per unit span is given by the following expressions

$$m_{\beta_l} = b(1 + c_l)\rho_f d_f, \quad m_{\beta_t} = b(1 - c_t)\rho_f d_f, \quad (11)$$

respectively. Flaps are treated as aerodynamically 'thin'.

Aerodynamic Model

The aerodynamic lift (L) and moments M , M^{β_l} and M^{β_t} used in expressions (5)-(8) are based on (Theodorsen and Garrick 1942), which makes use of thin aerofoil theory under an assumption of small amplitude oscillations of the wing-flap-tab system. This adopted configuration assumes that there is no fluid flow in the gaps between the wing and the aileron as well as between the aileron and the tab. Fluid flow of this kind however, could potentially improve the system performance, as has been established in aircraft applications. The transformation introduced in (Graham et al.

2011) is then employed for deriving the lift and moments acting on the deck-flaps combination.
The aerodynamic forces can thus be expressed in the following matrix form

$$F_{se} = M_{nc}\ddot{q} + C_{nc}\dot{q} + K_{nc}q + \Xi_C, \quad (12)$$

where q is the position vector defined as $q = \{h, \alpha, \beta_l, \beta_t\}^T$. The equations of motion of the sectional model (4-DOF deck-flap assembly), given by equations (5)-(8) in combination with the aerodynamic forces given in Eq.(12) are expressed in the following state space form:

$$\begin{bmatrix} 0 & M_s - M_{nc} \\ I & 0 \end{bmatrix} \begin{bmatrix} \dot{q} \\ \dot{q}_v \end{bmatrix} = \begin{bmatrix} -K_s & -C_s + C_{nc} \\ 0 & I \end{bmatrix} \begin{bmatrix} q \\ q_v \end{bmatrix} + \Xi_C \quad (13)$$

q_v is the velocity vector defined as $q_v = \{\dot{h}, \dot{\alpha}, \dot{\beta}_l, \dot{\beta}_t\}^T$. By introducing the state vector $x = \{q, q_v\}^T$, Eq.(13) can be expressed in the form:

$$E_c \dot{x} = A_c x + \Xi_C \quad (14)$$

where

$$E_c = \begin{bmatrix} 0 & M_s - M_{nc} \\ I & 0 \end{bmatrix} \quad A_c = \begin{bmatrix} -K_s + K_{nc} & -C_s + C_{nc} \\ 0 & I \end{bmatrix} \quad (15)$$

The matrices M_s, C_s, K_s are the system's structural matrices easily derived from equations (5)-(8). the matrices M_{nc}, C_{nc}, K_{nc} represent the non-circulatory part of the aerodynamic forces, usually referred to as added mass and damping component, whereas Ξ_C denotes the circulatory terms, which depend on the irrational Theodorsen function $C(ik)$, (Graham et al. 2011), and therefore cannot be expressed directly in a state space form. The non-circulatory flow contribution is computed using the aerodynamic expressions of the wing-flap-tab system, denoted as M_a, C_a, K_a , (Theodorsen and Garrick 1942), by transformation to the leading flap-deck-trailing flap mechanism using the following transformation matrix V :

219

$$M_{nc} = V^T M_a V \quad C_{nc} = V^T C_a V \quad k_{nc} = V^T K_a V \quad V = \begin{bmatrix} 1 & 0 & c_l b & 0 \\ 0 & 1 & -1 & 0 \\ 0 & 0 & 1 & 0 \\ 0 & 0 & 0 & 1 \end{bmatrix} \quad (16)$$

220

where

$$M_a = \rho b^4 \begin{bmatrix} -\frac{\pi}{b^2} & \frac{a\pi}{b} & \frac{-T_4(c_l)l + T_1(c_l)}{b} & \frac{-T_4(c_t)m + T_1(c_t)}{b} \\ \pi a^2 - \frac{\pi}{8} & -T_{24}(c_l)l - 2T_{13}(c_l) & -T_{24}(c_t)m - 2T_{13}(c_t) \\ sym & \frac{l^2 T_5(c_l) - 2l T_2(c_l) + T_3(c_l)}{\pi} & \frac{m Y_1(c_l, c_t) - l Y_3(c_l, c_t) - Y_4(c_l, c_t) + Y_6(c_l, c_t)}{\pi} \\ & \frac{m^2 T_5(c_t) - 2m T_2(c_t) + T_3(c_t)}{\pi} \end{bmatrix} \quad (17)$$

221

$$C_a = \rho b^3 U \begin{bmatrix} 0 & -\frac{\pi}{b} & \frac{2l\sqrt{-c_l^2 + 1} + T_4 c_l}{b} & \frac{2m\sqrt{-c_t^2 + 1} + T_4 c_t}{b} \\ 0 & a\pi - \frac{\pi}{2} & -T_{23}(c_l)l - T_{16}(c_l) & -T_{23}(c_t)m - T_{16}(c_t) \\ 0 & -T_{25}(c_l)l - T_{17}(c_l) & \frac{-T_{29}(c_l)l^2 - T_{27}(c_l)l - T_{19}(c_l)}{\pi} & \frac{-Y_{16}(c_l, c_t)lm - Y_{12}(c_l, c_t)l - Y_{14}(c_l, c_t)m - Y_{10}(c_l, c_t)}{\pi} \\ 0 & -T_{25}(c_t)m - T_{17}(c_t) & \frac{Y_{24}(c_l, c_t)m - Y_{22}(c_l)l - Y_{20}(c_l, c_t)m - Y_{18}(c_l, c_t)}{\pi} & \frac{-T_{29}(c_t)m^2 - T_{27}(c_t)m - T_{19}(c_t)}{\pi} \end{bmatrix} \quad (18)$$

222

$$K_a = \rho b^2 U^2 \begin{bmatrix} 0 & 0 & 0 & 0 \\ 0 & 0 & -T_{22}(c_l)l - T_{15}(c_l) & -T_{22}(c_t)m - T_{15}(c_t) \\ 0 & 0 & \frac{-T_{28}(c_l)l^2 - T_{26}(c_l)l - T_{18}(c_l)}{\pi} & \frac{-Y_{15}(c_l, c_t)lm - Y_{11}(c_l, c_t)l - Y_{13}(c_l, c_t)m - Y_9(c_l, c_t)}{\pi} \\ 0 & 0 & \frac{-Y_{23}(c_l, c_t)lm - Y_{21}(c_l, c_t)l - Y_{19}(c_l, c_t)m - Y_{17}(c_l, c_t)}{\pi} & \frac{-T_{28}(c_t)m^2 - T_{26}(c_t)m - T_{18}(c_t)}{\pi} \end{bmatrix} \quad (19)$$

223

$T_{ij}(\cdot)s, Y_{ij}(\cdot, \cdot)s, l$ and m were originally presented in (Theodorsen and Garrick 1942) and determine the aerodynamic effects of deck-flap hinge positions, whereas a denotes the distance from the chord midpoint to the section's rotation axis, for symmetric cross sections $a = 0$. The circulatory term Ξ_C of the aerodynamic forces can be expressed mathematically by the feedback-loop system in Fig.4, in which the approximation of the circulation function $C(s)$ is regarded as a transfer function receiving structural response $y = Q$ and generating output \tilde{y} , which finally translates into lift and moment aerodynamic forces by matrix B . This procedure is a convenient way of writing Theodorsen's equations and simultaneously performing a rational function approximation of the Theodorsen function. An equivalent state space realization $\tilde{A}, \tilde{B}, \tilde{C}, \tilde{D}$ of $C(s)$ is derived using standard techniques. The number of additional (aerodynamic) states is four, because $C(s)$ is of fourth order (Graham et al. 2011). The Q term is again deduced from the analytical framework in (Theodorsen and Garrick 1942), which after transformation into the leading-deck-trailing combination takes the following form:

$$Q = \dot{h} + U\alpha + \frac{1}{2}b\dot{\alpha} + \left[\frac{1}{\pi}T_{10}(c_l)U - U \right] \beta_l + \left[\frac{1}{2\pi}T_{11}(c_l)b + c_l b - \frac{1}{2}b \right] \dot{\beta}_l + \frac{1}{\pi}T_{10}(c_t)U\beta_t + \frac{1}{2\pi}T_{11}(c_t)b\dot{\beta}_t, \quad (20)$$

whereas

$$B = \begin{bmatrix} -2\pi\rho Ub & \pi\rho Ub^2 & -\{\pi + T_{12}(c_l) + 2\pi c_l\}\rho Ub^2 & -T_{12}(c_t)\rho Ub^2 & 0 & 0 & 0 & 0 \end{bmatrix}^T \quad (21)$$

The traditional approach to aeroelastic stability analysis is based on finding iteratively wind speed(s) for which sinusoidal solutions to equations (5) and (6) exist. Standard algorithms, including the k -method and the $(p - k)$ -method (Hodges and Pierce 2002), require the repeated evaluation of the Theodorsen function (Theodorsen 1934; Bisplinghoff et al. 1996). This approach has several disadvantages as has been explained in (Bakis et al. 2016; Graham et al. 2011), and thus it makes computational sense to employ a low-order rational function to approximate the circulation function. Approximations of this type allow one to formulate the problem in a state-space form and to use

analytic devices such as root-locus and Nyquist diagrams. The quartic approximation used in this work is defined as follows:

$$C(ik) = \frac{0.995 + 57.018(ik) + 23.788(ik)^2 + 1895.463(ik)^3 + 1523.247(ik)^4}{1 + 62.304(ik) + 807.784(ik)^2 + 3060.678(ik)^3 + 3033.763(ik)^4} \quad (22)$$

where $k = \frac{\omega b}{U}$ is the non-dimensional reduced frequency (ω is the oscillation frequency of the vibrating deck). The reduced frequency is also used as an indicator of flow unsteadiness (Bisplinghoff et al. 1996). The effectiveness of this approximation has been presented in (Graham et al. 2011; Bakis et al. 2016).

FEEDBACK SYSTEM

Feedback Configuration and Robustness Type

The block diagram of the bridge control system in Figure 5 demonstrates the interconnection of structural dynamics, fluid dynamics and the control system. The uncontrolled system is described by the plant $P(s)$ that contains the structural dynamics and the non-circulatory part of the fluid mechanics, while the Theodorsen function approximation $C(s)$ generates the circulatory flow. The controllers for the leading- and trailing- edge flaps are denoted by $K_l(s)$ and $K_t(s)$ respectively, and their function is to generate flap torques $M_c^{\beta_l}$ and $M_c^{\beta_t}$, from flap velocities, $\dot{\beta}_l$ and $\dot{\beta}_t$. Because the inputs and outputs of the plant are in different units, torques and angle rates respectively, a normalization factor has been implemented in the controller design process. Block diagrams of this sort are frequently used to assess both nominal and robust stability (Green and Limebeer 1995). In the control design exercise we presume an asymmetric configuration of the flaps as the prevailing wind direction for an individual bridge is usually known from site measurements. In a different case of course a symmetry restriction should be applied. The issue of flap controller symmetry has been recently discussed in (Zhao et al. 2011).

In the context of large civil engineering structures, many advantages derive from the use of passive controllers that require no power supply. The initial feedback control investigation will implement a standard mechanical layout, comprising of a spring and a damper at the hinged con-

nection of the leading and trailing flaps. Three hinge positions are considered, shown schematically in Figure 6. The flap width is considered constant at 2.75m and regarded as an internal part of the walkways, having width 3.25m.

The procedure for designing the mechanical elements, spring and damper, at the flap pivots is based on a constraint optimization procedure. The objective of the process is to maximize the robust stability margins in a sense to be described. The higher the stability robustness margin, the larger the uncertainties (e.g. variations in the model and/or in its parameters) under which the controlled system can remain stable. This is an essential requirement because ultimately it is the bridge and not the bridge model that needs to be stabilized. A key assumption in the modelling of the feedback system is that the uncertain part of the process is considered separate from the known nominal process model, unstructured uncertainty (McFarlane and Glover 1990). A variety of robustness criteria with respect to different unstructured uncertainty models can be postulated, e.g. robustness to an additive or multiplicative perturbation on the plant P , on the controller K on the loop transfer function, on the loop transfer function and so on. Note that the controller is assumed diagonal

$$K = \begin{bmatrix} K_l, 0 \\ 0, K_t \end{bmatrix},$$

generating flap torques $[M_c^{\beta_l}, M_c^{\beta_t}]^T$ from the flap velocities $[\dot{\beta}_l, \dot{\beta}_t]^T$. In this work we make use of additive perturbations on the normalized left coprime description of the plant, because it combines advantages from several different robustness criteria (Green and Limebeer 1995; Skogestad and Postlethwaite 2006). It can for instance account for uncertainties on lightly damped natural frequencies, which influence the system's dynamic behavior. It has been demonstrated that the representation of model errors as stable perturbations to the normalized coprime factors of the nominal plant model provides a more general description of the robust stability problem (McFarlane and Glover 1990). Optimizing for additive perturbation on the plant P is known to give controllers with poor gain margins but places a favourable explicit limit on the high-frequency gain of the resulting controller. On the other hand, an index related to multiplicative perturbation on

P is known to give good robustness margin, but may have unbounded high-frequency gain (Bakis et al. 2016).

The normalized left coprime factorization of the plant P is defined as follows:

$$P = N_L^{-1} N_R \quad (23)$$

where $N_L, N_R \in H_\infty$ and

$$N_L N_L^\sim + N_R N_R^\sim = I \quad (24)$$

where $(\cdot)^\sim$ means adjoint. The perturbed plant is:

$$P_\Delta = (N_L - \Delta_{N_L})^{-1} (N_R + \Delta_{N_R}) \quad (25)$$

The aim is to design a stabilizing controller that maximizes the size of admissible perturbation:

$$\left\| \begin{bmatrix} \Delta_{N_L} & \Delta_{N_R} \end{bmatrix} \right\|_\infty < \gamma^{-1} \quad (26)$$

thereby minimizing the achievable value of γ (Green and Limebeer 1995; Skogestad and Postlethwaite 2006):

$$\left\| \begin{bmatrix} K \\ I \end{bmatrix} (I - PK)^{-1} \begin{bmatrix} P & I \end{bmatrix} \right\|_\infty < \gamma = \frac{1}{\epsilon} \quad (27)$$

In practice the objective is to find a stabilizing feedback controller that minimizes the robustness index γ while satisfying Eq.(27) (ϵ is called normalized coprime stability margin or gap metric stability margin). Note that it is always $\gamma \geq 1$. It is worth noting that minimizing γ results in a bounded ∞ -norm for KS, S, KSP, SP (these terms are the four sub-matrices obtained when expanding the left hand side of Eq.(27)), where $S = (I - PK)^{-1}$. These terms are robust stability indexes: the lower their norm, the better the related robustness. In particular $\|KS\|_\infty$ is related to the robustness against additive perturbation on the plant P , $\|S\|_\infty$ is related to the robustness against additive perturbation on the loop transfer function PK , $\|KSP\|_\infty$ is related to the robustness

against multiplicative perturbation on the controller K and $\|SP\|_\infty$ is related to the robustness against additive perturbation on controller K .

Stability Analysis and Robustness Characteristics

Following the procedure with regards to stability presented in (Omenzetter et al. 2000b; Graham et al. 2011; Bakis et al. 2016), we present the root-locus for the open-loop system in Figure 7, which effectively consists of the eigenvalues of generalized state space model at different wind speeds. Since the system is uncontrolled the flaps are considered rigidly attached to the deck. The wind speed is varied between 0 m/s and 90 m/s. Pitch-mode flutter occurs at a wind speed of 65 m/s, when the real part becomes positive, while the torsional divergence mode becomes unstable at 72 m/s (Graham et al. 2011). While flutter is a divergent oscillatory mode, torsional divergence is an aeroelastic mode that derives from the wind-induced twisting moment applied to the bridge deck by the lift force acting close to the quarter chord (Hodges and Pierce 2002). Torsional instability results when this moment overcomes the restoring moment due to the deck's torsional stiffness.

Optimization I: spring-damper on hinges

An optimization process is next performed for each of the three configurations presented in Fig. 6. The stiffness and damping at the flap hinges are the sought after optimization parameters, whereas the optimization objective is the minimization of γ in Eq. (27), constraint to closed-loop system stability. A fully symmetric configuration is initially assumed, i.e. same values of spring/damper and hinge location for the windward and leeward sides. The optimization results demonstrate that case 3 exhibits the most favourable aeroelastic characteristics, with both the critical flutter speed and divergence speed significantly increased. For case 1 the optimized retention components yield an effectively rigid connection between the flaps and deck; consequently, softening of the springs results in lower critical wind speeds. The comparison of the stability behavior for the three cases is presented by the root-loci diagrams in Fig. 8 and the optimization results are summarized in Table 2.

As was highlighted in the previous section the choice of the robustness index based on the coprime realization of the system is founded on the premise that this is related to physical properties

of the model. Consequently, it is anticipated that the deck-flap configuration of case 3, having a smaller robustness index or equivalently a large stability margin index, will be less sensitive to variations when compared to case 2. However, it should be stressed that the equivalence between robustness index and allowable tolerance in parametric variations is not proportional. This is expected since the modelling follows an unstructured representation for the uncertainty process. To further illustrate this point, cases 2 and 3 are examined in terms of the closed loop system's stability while reducing the torsional natural frequency in a vacuum. The choice of torsional frequency as the varied parameter is due to its dominant contribution to the flutter mode. Fig. 9 demonstrates that case 3 can in fact sustain slightly larger reduction in the bridge's torsional stiffness. Both cases however exhibit a type of soft flutter behavior when relatively minor changes to the deck's torsional stiffness are introduced. It should be pointed out that the optimization objective, which namely consists in maximizing the controlled system's stability margin, is evaluated at increasing wind speeds. The robustness indexes presented in Table 2 capture the worst case scenario. However the system's damping at different wind speeds can be deteriorated when compared to another case with lower worst case robustness. Fig. 8 for example shows that case 1 has slightly more damping (which is related to the distance from the imaginary axis) for the pitch mode at lower wind speeds compared to cases 2 and 3.

Optimization II: compensator in parallel to spring-damper on hinges

The control investigation described in the previous section demonstrated that a significant increase in aeroelastic boundaries can be achieved through the combination of optimized flap retention components and optimized deck-flap pivot location. The spring and damper elements optimized are effectively the structural parameters K_{β_l} , K_{β_t} as well as C_{β_l} , C_{β_t} in equations (5)-(8). The location of the flap hinges is implemented in the model by computing the structural quantities in equations (9)-(10) as well as adjusting the l and m parameters, which determine the aerodynamic effects of the hinge position, in equations (17)-(19). The main disadvantage of this relatively simple feedback mechanism is the resulting poor robustness properties. The following examination seeks to improve the stability margins, while retaining the increased critical flutter and divergence

speeds, by introducing control networks $K_l(s)$ and $K_t(s)$ in parallel to the retention components. In this study we confine our attention to passive control systems that require no power supply. Consequently, the additional feedback system should be realized by the interconnection of passive mechanical components. It is worth stressing that the network layout is not preselected. Instead, a passivity constraint is assigned to the controller transfer function and a mechanical realization is then derived based on springs, dampers and inerters (Bott and Duffin 1949; Smith 2002). The inerter element bridges the gap in establishing an electrical-mechanical analogy which would allow the full implementation of the electrical circuit synthesis theory for mechanical systems. An inerter provides a force proportional to the acceleration difference between its two terminals, with the constant of proportionality termed the inertance, say b . Working in terms of angular motion, b relates torque to angular acceleration and so has units of kgm^2 . Mechanically geared inerters have been constructed using a flywheel, rack, pinion and gears, see e.g. Fig.3 (Smith 2002). Note that such a device does not have the limitation that one of the terminals be grounded.

The theory of passive networks has been widely studied in the electrical engineering literature (Anderson and Vongpanitlerd 1973), and is based on the idea of through and across variable. The concept of passivity can be translated directly to mechanical networks as follows: A mechanical one-port network with a force-velocity pair (F, v) , see Fig. 10, is defined as passive if for all admissible F and v , square integrable over $(-\infty, T)$, Eq. (28) is satisfied.

$$\int_{-\infty}^T F(t)v(t)dt \geq 0 \quad (28)$$

It can be shown (Newcomb 1966; Anderson and Vongpanitlerd 1973) that a rational transfer function relating the through variable and the across variable is passive if it is positive-real, i.e. if it is stable and with positive real part.

In the examined deck-flap system, whose block diagram is presented in Fig. 5, the through variables are the flap torques $M_c^{\beta_l}$, $M_c^{\beta_t}$, see equations (7)-(8), and the cross variables are the flap angle rates $\dot{\beta}_l$, $\dot{\beta}_t$. Consequently the leading and trailing flap compensator admittance functions are defined as $K_l(s) = M_c^{\beta_l} / \dot{\beta}_l$ and $K_t(s) = M_c^{\beta_t} / \dot{\beta}_t$ respectively. The higher the order of the (two-

terminal) compensator, the larger the number of mechanical elements (springs, dampers, inerters) that must be used (in series and/or parallel) to generate such compensator. It can be shown that only three elements are necessary to realize any first order passive network, while five to eight elements are necessary to realize any second order passive network (Jiang and Smith 2011; Jiang and Smith 2012; Hughes and Smith 2014). For simplicity of implementation we concentrate on first order compensators for the flap controllers that seek to further reduce the robustness index obtained in the previous section. To ensure that the optimization problem is properly posed a number of constraints must be put in place that operate alongside.

1. In order to ensure stability, the closed-loop eigenvalues are constrained to have negative real parts.
2. The compensators' gains are constrained so that high ratio gearboxes and/or levers, and flow separation are avoided.
3. The compensators are constrained to be passive so that they can be synthesized using passive mechanical components (springs, dampers and inerters) (Smith 2002). This is ensured by imposing a positive-real constraint on the compensator coefficients (Papageorgiou and Smith 2006).

The design results of this procedure for cases 2 and 3, see Fig. 6 are presented in Table 3. The final flap controllers consist of a spring and a damper in parallel to the mechanical realization of $K_l(s)$ and $K_t(s)$. The overall system admittance is denoted as $Y_{gl}(s)$ and $Y_{gt}(s)$ for the leading and trailing flaps respectively. The transfer functions of the flap controllers are also included, as well as the allowable variations of the zero wind speed natural torsional frequency. Case 1 is not reported because no improvement was obtained when using an additional compensator. For case 3 a trade-off between the maximum critical flutter speed and the allowable robustness is presented (cases 3a and 3b). Clearly, by introducing a first order compensator at the deck-flap hinges we can significantly raise the system's tolerance to parametric uncertainty in the torsional frequency. Similar results are attained for variations in aerodynamic parameters. Design analysis using second

order passive compensators was also conducted, but the improvement in robust performance over the first-order one was marginal.

In order to synthesise the controller, one recalls that the admittance (the ratio force/velocity) of a damper is constant, say c . The admittance of a spring is k/s and the admittance of an inerter is bs (Smith 2002). Therefore, if one were to consider a damper and spring connected in parallel, the admittance of the combination would be $c + k/s$. Applying the basic rules associated with series and parallel combinations of mechanical elements, the admittance is the sum of the admittances for a parallel combination of elements, while the inverse of the sum of the inverses is used for a series combination. In the case of the first-order compensator (29), one observes that when $\hat{A}\hat{D} - \hat{B}\hat{C} > 0$:

$$\begin{aligned} K(s) &= \frac{\hat{A}s + \hat{B}}{\hat{C}s + \hat{D}} = \left(\frac{\hat{C}s + \hat{D}}{\hat{A}s + \hat{B}} \right)^{-1} = \left(\frac{\hat{C}}{\hat{A}} + \left(\frac{\hat{A}(\hat{A}s + \hat{B})}{\hat{A}\hat{D} - \hat{B}\hat{C}} \right)^{-1} \right)^{-1} = \\ &= \left(\frac{1}{\hat{A}/\hat{C}} + \left(\frac{\hat{A}^2s}{\hat{A}\hat{D} - \hat{B}\hat{C}} + \frac{\hat{A}\hat{B}}{\hat{A}\hat{D} - \hat{B}\hat{C}} \right)^{-1} \right)^{-1} = \left(\frac{1}{c_1} + (bs + c_2)^{-1} \right)^{-1} \end{aligned} \quad (29)$$

which represents a damper $c_1 = \hat{A}/\hat{C}$ connected in series with the parallel combination of a damper $c_2 = \hat{A}\hat{B}/(\hat{A}\hat{D} - \hat{B}\hat{C})$ and an inerter $b = \hat{A}^2/(\hat{A}\hat{D} - \hat{B}\hat{C})$; see Fig. 11.

It is noted that in the case $\hat{A}\hat{D} - \hat{B}\hat{C} < 0$ a different network layout is found. Indeed it is

$$\begin{aligned} K(s) &= \frac{\hat{A}s + \hat{B}}{\hat{C}s + \hat{D}} = \frac{\hat{A}}{\hat{C}} + \frac{\hat{B}\hat{C} - \hat{A}\hat{D}}{\hat{C}(\hat{C}s + \hat{D})} = \frac{\hat{A}}{\hat{C}} + \left(\frac{\hat{C}^2s}{\hat{B}\hat{C} - \hat{A}\hat{D}} + \frac{\hat{C}\hat{D}}{\hat{B}\hat{C} - \hat{A}\hat{D}} \right)^{-1} \\ &= \frac{\hat{A}}{\hat{C}} + \left(\frac{1}{\frac{\hat{B}\hat{C} - \hat{A}\hat{D}}{\hat{C}^2s}} + \frac{1}{\frac{\hat{B}\hat{C} - \hat{A}\hat{D}}{\hat{C}\hat{D}}} \right)^{-1} = c_1 + \left(\frac{1}{\frac{k}{s}} + \frac{1}{c_2} \right)^{-1} \end{aligned}$$

which consists of a damper $c_1 = \hat{A}/\hat{C}$ in parallel with the series connection of a spring $k = (\hat{B}\hat{C} - \hat{A}\hat{D})/\hat{C}^2$ and a damper $c_2 = (\hat{B}\hat{C} - \hat{A}\hat{D})/\hat{C}\hat{D}$.

As a final remark, it is noted that the two networks discussed are able to replicate all first order passive transfer functions. First order transfer functions are a special case of biquadratics, whose properties and synthesis are discussed in (Jiang and Smith 2011).

The physical parameters of the networks for the different transfer functions presented in Table 3 are shown in Table 4. For cases 2 and 3b, the magnitude of the damper c_2 is considerably smaller

than that of c_1 , so without loss in performance the transfer function can be realized using just an inerter and damper in series.

The time response of the previously optimized deck-flap system is next investigated. The aim is to examine the effectiveness of the passive flap mechanism in suppressing the deck's divergent pitching and heaving motion at different wind speeds. The corresponding flap movement is also observed. The deck's pitch transient response as well as the associated flap rotation is presented in Fig. 12 for wind speeds of 75m/s and 85m/s, given a $2\text{deg}=0.035\text{rad}$ deck pitch initial condition. It is shown that the rotation of the leading and trailing flaps is comparable and that their magnitude is restrained below $0.07\text{rad}=4\text{deg}$ for wind speeds up to 85m/s, for the given initial condition. Consequently, the resulting flap angles are considerably below flow separation limits caused by flap movement (Gouder et al. 2015). Further details on the system's performance comparison to an active power driven H_∞ control framework (Bakis et al. 2016), is given in (Bakis 2016), along with further investigation on the separate influence of the leading and trailing flaps.

Section summary

This section addressed the problem of stabilizing aeroelastic instabilities in a bridge-section model using a passive control scheme. An optimization process is proposed for tuning the values of the mechanical components, which connect the flaps to the deck. Best results in terms of stability and robustness are achieved when the connection is at the outer edge of the flaps, case 3. In the case where the optimization parameters are only a spring and a damper at the connection, significant improvement in the critical flutter speed and divergence speed is gained but the robustness of the system is poor. We are able to improve robustness properties of the system by introducing a first order compensator in parallel with the spring-damper. The mechanical realization of these compensators also introduces the use of the inerter, which appears to have a considerable impact on the system's aeroelastic properties. The proposed mechanical configuration is also quite simple to implement in real bridge structures as it avoids the use of additional structural components such as supporting beams or pendulums (Omenzetter et al. 2000a; Wilde et al. 1999; Phan and Nguyen 2013).

A NEXUS BETWEEN TUNED DAMPERS AND FLAPS

In this section the Tuned Mass Damper's (TMD) properties are exploited in order to control aerodynamic surfaces adjacent to the deck. The combined system is referred to as the *flap mass damper* (FMD). It is shown that this novel approach can significantly improve the aeroelastic limits while achieving good robustness margins, as well as limiting rotations of the flaps and vertical movement of the suspended masses. The function of the tuned mass in this case is twofold. Firstly, the motion of the masses is related to the deck's heaving and pitching movement and consequently it consists of an indirect way of sensing the input signal for the flap controllers. The proposed linkage between the tuned masses and the flaps relates to the inherent problem of passive systems based on flaps associated with lack of access to a ground reference point. Consequently, flap rotation cannot be explicitly linked to deck movement. The tuning procedure of the TMD in essence establishes the feedback relationship between the two components, flaps and TMDs, and a virtual ground connection is achieved. Secondly, the oscillating masses provide driving forces for controlling flap rotation. In general it is expected that the flap which is subjected to larger aerodynamic force will require a bigger mass connected to it.

Review of Tuned Mass Dampers (TMDs)

This section reviews some of the characteristics and shortcomings of using an eccentric mass or TMDs for suppressing aeroelastic instabilities. We make use of the previous sectional model of the Humber Bridge, which now considers the flaps to be rigidly attached to the deck, see Fig. 13. Aerodynamic analysis is similar to that of the previous section.

A special case of the deck-TMD system is when an eccentric mass is placed on the windward deck side, referring to Fig. 13 this translates to $m_{dr} = 0$. Furthermore, it is assumed that $K_{dl} \rightarrow \infty$. The underlying physical principle involved in flutter control by using an eccentric ballast is the reduction of aerodynamic moment, acting on the deck's center of rotation (Larsen 1997). Fig. 14 presents the root-loci with the wind speed U being the varied parameter for a range of mass ratios μ , defined as $\mu = \frac{m_{dl}}{m}$, as well as the corresponding instability mode. For example, in the case of an added mass ratio of $\mu = 0.1$, which corresponds to an eccentric mass of 1.32t/m, the flutter

boundary is raised from 65m/s to 75m/s. It becomes clear that this methodology, although simple, provides only modest improvement to the critical flutter speed and fails to substantially raise the critical divergence speed. In addition our analysis showed that the achieved stability margins are small.

Returning to the twin-TMD arrangement, Fig. 13, the following investigation will concentrate on implementing a non-linear optimization process for tuning the physical parameters of the two tuned masses. The system has now four degrees of freedom, namely: deck heave, deck pitch and the two vertical displacements of the two TMD masses relative to the deck, h_{dl} and h_{dr} . The optimization parameters are the mass, stiffness and damping of each TMD: m_{dl} , K_{dl} , ζ_{dl} , m_{dr} , K_{dr} and ζ_{dr} . Two cases are examined; the first, case TMD1, allows a maximum left mass ratio index of $\mu_{l,max} = \frac{m_{dl}}{m_d} = 0.07$ and maximum right mass ratio of $\mu_{r,max} = \frac{m_{dr}}{m_d} = 0.035$. The second case, case TMD2, considers both $\mu_{l,max} = \frac{m_{dl}}{m_d} = 0.07$ and $\mu_{r,max} = \frac{m_{dr}}{m_d} = 0.07$. The optimization objective, similarly to the previous case is to maximize the normalized coprime stability margin. Large movements of the tuned mass are also penalized by introducing weighting coefficients for minimizing the TMDs natural periods, T_{dl} and T_{dr} . Hence, the optimization objective reads

$$\min_{m_{dl/r}, K_{dl/r}, \zeta_{dl/r}} \{0.5\|\gamma\|_{\infty} + 0.25T_{dl} + 0.25T_{dr}\}. \quad (30)$$

The optimization framework implemented resulted, in this case, in a mechanical deck-TMD configuration, in which the windward mass is almost static, see Fig. 15. The windward mass consequently performs a function similar to that of an eccentric mass whereas the leeward mass exhibits considerable oscillatory motion. Previous studies which have addressed the effectiveness of auxiliary dampers in controlling bridge flutter have used simplified formulas for tuning the mechanical components. For our system implementing these formulas gave very comparable performance in terms of aeroelastic limits although the two procedures resulted in different estimations for the TMD mechanical properties. It is worth noting that the derived optimal TMD parameters result in optimal performance when the negative damping related to the self-excited motion equals the

maximum damping $(\xi_s)_{max}$ for the given TMD ratio, meaning that the TMD parameters are chosen to change the negative damping of the structure to zero for a given wind speed. As was pointed out in (Chen and Kareem 2000) this is a very limiting case as in real life applications it is expected that the designed TMD mass ratio, tuning frequency and damping ratio achieve maximum positive damping for the deck-TMD system. Alternative formulas have been proposed to overcome this issue by Chen and Kareem (Chen and Kareem 2000), however in every case the TMD performance is very sensitive to the tuning frequency and damping ratio.

This rather concise review on TMD implementation in controlling self-excited motion exposed some of the inherent shortcomings of this methodology. It was shown that TMDs are unsuccessful in increasing the torsional divergence boundary. This is an important drawback as it is often the case that flutter critical wind speed is close to the divergence limit, e.g. Humber Bridge. The suspended masses also experience large displacements, TMD stroke, relative to the deck, particularly in the leeward side. It has also been shown that TMD performance is sensitive to design parameter tuning around their optimal values, which poses a significant limitation in terms of the system's robustness. The presented design will serve as a building block for the following analysis, in which a kinematic constraint between the mass dampers and flaps is introduced. It was demonstrated that passive flaps can favorably modify the system's aerodynamic characteristics which effectively reduces the rate of change of modal damping with increasing wind velocity, also referred as soft-flutter, whereas the auxiliary damped masses control the flap movement and provide additional damping.

Passive Control with Movable flaps and kinematically connected TMD (Flap Mass Damper)

A combined system of symmetrically suspended masses connected to the flap controllers is here proposed, referred to as the flap mass damper (FMD) Fig. 16. For deriving the equations of motion Lagrange's approach is again employed, see Eq.(1). Additional terms to the kinetic energy T , potential energy V , and dissipation function D presented in equations (5)-(8), should be

considered due to the contribution of added suspended masses. These are respectively:

$$T_a = \frac{1}{2} \left(m_{dl} (\dot{h} - d_{tm}\dot{\alpha} + \dot{h}_{dl})^2 + m_{dr} (\dot{h} + d_{tm}\dot{\alpha} + \dot{h}_{dr})^2 \right), \quad (31)$$

$$V_a = \frac{1}{2} (K_{dl}h_{dl}^2 + K_{dr}h_{dr}^2), \quad D_a = \frac{1}{2} (C_{dl}\dot{h}_{dl}^2 + C_{dr}\dot{h}_{dr}^2). \quad (32)$$

The kinematic constraint between the tuned mass and the flap angle can be realized in different ways, for example through a rack, pinion and belt mechanism or by a connection using levers and a gear box. A conceptual realization of the proposed mechanism is graphically presented in Fig. 16. In this design, the TMD movement is transmitted through a rack-pinion-belt linkage. For the leading-edge flap a single pinion of radius r_o is used and for the trailing flap two pinions are needed in order to reverse the angle. Assuming radii of the pinions at the flap pivots r_l and r_t , it is computed that $h_{dl} = \beta_l \times r_l$ and $h_{dr} = -\beta_t \times r_t$. The sign for the latter expressions was determined after preliminary numerical investigations, which resulted in optimum performance for the chosen combination. For the current analytic investigation, however, it is only of essence to determine the kinematic relationship between the mass's vertical movement and the flap's rotation.

$$m_f \ddot{h} + (S_\alpha - m_{dl}d_{tm} + m_{dr}d_{tm})\ddot{\alpha} + (S_{\beta_l} + m_{dl}r_l)\ddot{\beta}_l + (S_{\beta_t} - m_{dr}r_t)\ddot{\beta}_t + C_h\dot{h} + K_h h = L, \quad (33)$$

$$(S_\alpha - m_{dl}d_{tm} + m_{dr}d_{tm})\ddot{h} + I_f \ddot{\alpha} - (I_{\beta_l} - r_{\beta_l}S_{\beta_l} + m_{dl}r_ld_{tm})\ddot{\beta}_l + (I_{\beta_t} + r_{\beta_t}S_{\beta_t} - m_{dr}r_td_{tm})\ddot{\beta}_t + C_\alpha \dot{\alpha} + K_\alpha \alpha = M, \quad (34)$$

$$(S_{\beta_l} + m_{dl}r_l)\ddot{h} - (I_{\beta_l} - r_{\beta_l}S_{\beta_l} + m_{dl}r_ld_{tm})\ddot{\alpha} + (I_{\beta_l} + m_{dl}r_l^2)\ddot{\beta}_l + (C_{\beta_l} + r_l^2C_{dl})\dot{\beta}_l + (K_{\beta_l} + r_l^2K_{dl})\beta_l = M_l^\beta + M_c^{\beta_l}, \quad (35)$$

$$(S_{\beta_t} - m_{dr}r_t)\ddot{h} + (I_{\beta_t} + r_{\beta_t}S_{\beta_t} - m_{dr}r_td_{tm})\ddot{\alpha} + (I_{\beta_t} + m_{dr}r_t^2)\ddot{\beta}_t + (C_{\beta_t} + r_t^2C_{dr})\dot{\beta}_t + (K_{\beta_t} + r_t^2K_{dr})\beta_t = M^{\beta_t} + M_c^{\beta_t}, \quad (36)$$

where $m_f = m_d + m_{\beta_l} + m_{\beta_t} + m_{dl} + m_{dr}$ and $I_f = I_a + m_{dl}d_{tm}^2 + m_{dr}d_{tm}^2$. The expressions for aerodynamic lift L and the aerodynamic moments M , M^{β_l} , M^{β_t} follow the same formulation

567 developed in the previous sections.

568 In terms of the mechanical network at the flap pivot point, different alternatives of increasing
569 complexity were investigated. It was again observed that using a first order compensator in parallel
570 to structural flap retention components resulted in the simplest network with marginally worse
571 performance when compared to higher order compensators. Referring to Fig. 5 the flap angular
572 rates $\dot{\beta}_l, \dot{\beta}_t$ are the inputs to the compensators, which in turn produce the flap torques $M_c^{\beta_l}$ and
573 $M_c^{\beta_t}$ as outputs. in Fig. 16 the mechanical compensators are denoted by $K_l(s)$ and $K_t(s)$ for the
574 leading and trailing flap respectively. The number of optimization parameters is 14, 2×4 for
575 the compensators at the flap pivot plus 6 parameters for the mechanical components of the mass
576 dampers. Similarly to section 3, the objective is to minimize the robustness index and to constrain
577 the controllers $K_l(s)$ and $K_t(s)$ to be passive. Table 6 summarizes the mechanical components
578 of the FMD for 3 hinge locations whereas Table 7 presents the key findings related to aeroelastic
579 stability limits and robustness properties.

580 Comparing the analysis results of Table 7 to those of Table 3, it can be concluded that adding
581 an auxiliary TMD kinematically connected to the flaps significantly increases the flutter critical
582 wind speed. For cases 1 and 2 the critical divergence speed poses a limit on the possible increase.
583 Moving the hinge on the outer edge for the leading flap as in Case 3 alters the aerodynamics in a
584 favorable way and increases the divergence limit making it possible to achieve better aerodynamic
585 performance with good robustness margins. Moreover, when the aeroelastic stability limit is posed
586 by the divergence limit, smaller tolerance to torsional stiffness variations is attained. This is to be
587 expected, because the torsional divergence, being an aerostatic instability mode, is directly related
588 to the deck's torsional stiffness. For suppressing this phenomenon the flap controllers would need
589 to produce a counter-balancing moment force, which would in turn translate to a non-zero flap
590 angle offset. However, it becomes clear that when structural stiffness decreases the robustness of
591 the control law is undermined. In Fig. 17 we show the Root Loci for the case 3b of Table 3 and
592 case 3 of Table 7. It is shown that the FMD results in better stability properties for the closed loop
593 system.

Fig. 18 presents the transient response of the deck heave, deck pitch and flap rotations for the three methodologies described in this paper for a wind speed $U=76\text{m/s}$. It is seen that similar transient behavior of the deck is attained and that the FMD exhibits slightly smaller flap rotations compared to the case when only movable flaps are present. At this point the reader is reminded that our analysis is based on thin airfoil theory and larger gains for the trailing flap might be required due to flow separation caused by deck bluntness. Indeed separation reduces the effectiveness of flaps, i.e. less force is produced per unit flap rotation. In (Gouder et al. 2015) it was concluded that a factor 2 to 3 on the movement of the trailing flap is needed in order to balance the effect of separation. This finding however, did not pose a serious issue as the flap angle never exceeded 6° . In Fig. 19 we demonstrate the mass movement of the mass dampers given an initial condition for the cases TMD2 and case 3 of Table 7. It is worth stressing that the FMD case results in much lower vertical movements of the suspended mass than the TMD alone, thus advocating for the applicability of the solution.

As already stressed, TMD parametric tuning sensitivity poses a serious reliability issue. Fig. 20(b) presents the FMD's effectiveness over tuning frequency variations of the leeward suspended mass, which is the most important. Compared to the equivalent TMD graph of Fig. 20(a) it is clearly illustrated that the FMD's performance is much less sensitive to optimal tuning of mechanical components. The presented optimization framework determined the tuning frequency of the right mass to be $\omega_{dr} \approx 12.75 \text{ rad/s}$. From the following figure it is seen that this value is a trade-off between achieved performance and robustness. The loss in robustness is explained by the steep drop in flutter boundaries at frequencies greater than $\omega_{dr} \approx 13.75 \text{ rad/s}$. This behaviour is due to a change in the flutter mode which becomes unstable for this choice of tuning parameters.

CONCLUSION

This paper analytically investigated the improved aeroelastic performance of three passively controlled mechanical networks. It was shown that the implementation of single tuned mass dampers is laced with problems associated to poor robustness margins and large movement of the suspended masses. On the contrary, solutions based on movable flaps, show great promise. The

first approach is based on a kinematic deck-flap arrangement, where an optimization process is used for tuning the mechanical components at the flap pivot points. It was shown that locating the flap hinges at the flap outer edges while optimizing for the flap retention components increases aeroelastic stability. Addition of a passive first order compensator, including inerter components, helps achieve better robustness properties.

The second approach focused on combining the benefits of tuned mass dampers systems with that of optimum flap kinematics. A transmission system designed out of purely passive components (spring, dampers and inerters) aims at achieving maximum robustness margins to structural uncertainties. The proposed design avoids the inherent shortcomings of TMDs while increasing flap effectiveness by providing additional structural damping. An advantage of both procedures is that the network layout is not preselected, but determined through an optimization process. The introduced flap mass damper network leads to a more more complicated design, but avoids external structural linkages which can pose serious technical difficulties as well as altering the deck's aerodynamic properties.

ACKNOWLEDGEMENTS

This work was partially funded by the IKY-State Scholarship Foundation by means of the ESPA European fund 2007-2013 and supported by a Marie Curie Intra European Fellowship within the 7th European Community Framework Programme.

REFERENCES

- Anderson, B. D. O. and Vongpanitlerd, S. (1973). *Network Analysis and Synthesis*. Prentice-Hall,Engelwood Cliffs, NJ.
- Bakis, K. N. (2016). "Active and passive aeroelastic control of long-span suspension bridges." Ph.D. thesis, University of Oxford, Department of Engineering Science, University of Oxford, Department of Engineering Science.
- Bakis, K. N., Massaro, M., Williams, M. S., and Limebeer, D. J. N. (2015). "Aeroelastic control

of long span suspension bridges during erection.” *IABSE conference, Elegance in Structures*,
Nara, Japan.

Bakis, K. N., Massaro, M., Williams, M. S., and Limebeer, D. J. N. (2016). “Aeroelastic control
of long-span suspension bridges with controllable winglets.” *Journal of Structural Control and
Health Monitoring*.

Billah, K. Y. and Scanlan, R. H. (1991). “Resonance, Tacoma Narrows bridge failure, and under-
graduate physics textbooks.” *American Journal of Physics*, 59(2), 118–124.

Bisplinghoff, R. L., Ashley, H., and Halfman, R. L. (1996). *Aeroelasticity*. Dover Publications,
New York.

Boberg, M., Feltrin, G., and Martinoli, A. (2015). “Flutter suppression of a bridge section model
endowed with actively controlled flap arrays.” *Intelligent Robots and Systems (IROS)*.

Bott, R. and Duffin, R. J. (1949). “Impedance synthesis without use of transformers.” *J. Appl. Phys.*,
20.

Chen, X. and Kareem, A. (2000). “Efficacy of tuned mass dampers for bridge flutter control.”
Journal of Structural Engineering ASCE, 129, 1291–1300.

Den Hartog, J. P. (1985). *Mechanical Vibration*. Dover, New York.

Diana, G., Federico, C., Alberto, Z., Colina, A., and Bruni, S. (1998). “Aerodynamic design of
very long-span suspension bridges.” *Long-Span and High-Rise Structures, IABSE Symposium*,
Kobe, 115–130.

Fujino, Y. and Abe, M. (1993). “Design formulas for tuned mass dampers based on a perturbation
technique.” *Earthquake Engineering and Structural Dynamics*, 22, 833–855.

Gimsing, N. J. (1997). *Cable Supported Bridges*. John Wiley & Sons.

Gouder, K., Zhao, X., Limebeer, D. J. N., and Graham, J. M. R. (2015). “Experimental aerody-
namic control of a long-span suspension bridge section using leading- and trailing- edge control
surfaces.” *IEEE Transactions on Control System Technology*, PP, 99, 1–13.

Graham, J. M. R., Limebeer, D. J. N., and Zhao, X. (2011). “Aeroelastic control of long-span
suspension bridges.” *Journal of Applied Mechanics*, 78, 041018–1 to 041018–12.

- Green, M. and Limebeer, D. J. N. (1995). *Linear Robust Control*. Prentice Hall, Englewood Cliffs, New Jersey.
- Hansen, H. I. and Thoft-Christensen, P. (2001). "Active flap control of long suspension bridges." *Journal of Structural Control*, 8(1), 33–82.
- Hodges, D. H. and Pierce, G. A. (2002). *Introduction to structural dynamics and aeroelasticity*. Cambridge Aerospace Series.
- Hughes, T. and Smith, M. (2014). "On the minimality and uniqueness of the Bott-Duffin realization procedure." *IEEE Trans on automatic control*, 59(7).
- Jiang, J. and Smith, M. (2011). "Regular positive-real functions and five element network syntnthesis for electrical and mechanical networks." *IEEE Trans. Automatic Control*, 56(6), 1275–1290.
- Jiang, J. and Smith, M. (2012). "Series-parallel six-element synthesis of biquadratic impedances." *IEEE Trans on Circuits and Systems-I*, 59(11).
- Kwon, S. and Park, K. (2004). "Suppression of bridge flutter using tuned mass dampers based on robust performance design." *Journal of Winf Engineering and Industrial Aerodynamics*, 92, 919–934.
- Kwon, S. D., Jung, M. S. S., and Chang, S. P. (2000). "A new passive aerodynamic control method for bridge flutter." *Journal of Wind Engineering and Industrial Aerodynamics*, 86, 187–2002.
- Larsen, A. (1997). "Prediction of aeroelastic stability of susepnson bridges during erection." *Journal of Wind Engineering and Industrial Aerodynamics*, 72, 265–274.
- Larsen, A., Vejrum, T., and Esdahl, S. (1998). "Vortex models for aeroelastic anlaysis assessment of multielement brdge decks." *Bridge aerodynamics, Larsen&Esdahl*, Balkema, Rotterdam.
- Li, K., Ge, Y. J., Guo, Z. W., and Zhao, L. (2015). "Theoretical framework of feedback aerodynamic control of flutter oscillation for long-span suspension bridges by the twin-winglet system." *Journal of Wind Engineering and Industrial Aerodynamics*, 145, 166–177.
- Lin, Y. Y., Cheng, C., and Lee, C. (2003). "A tuned-mass damper for suppressing the coupled flexural and torsional buffeting response of long-span bridges." *Journal of Engineering Structures*, 22, 1195–1204.

- Makoto, K. (2004). "Technology of the Akashi Kaikyo bridge." *Journal of Structural Control and Health Monitoring*, 11, 75–90.
- Massaro, M., Bakis, K. N., Limebeer, D. J. N., and Graham, M. J. R. (2015). "Flutter and buffeting of long span suspension bridges in fully erected and partially erected conditions." *International Forum on Aeroelasticity and Structural Dynamics*, Saint Petersburg, Russia.
- McFarlane, D. C. and Glover, K. (1990). *Robust Controller Design Using Normalized Coprime factor Plant Descriptions*. Lecture Notes in Control and information Sciences, 138, Springer-Verlag Berlin, Heidelberg.
- Newcomb, R. W. (1966). *Linear Multiport Synthesis*. McGraw-Hill.
- Omenzetter, P., Wilde, K., and Fujino, Y. (2000a). "Suppression of wind-induced instabilities of a long span bridge by a passive deck-flaps control system part I: Formulation." *Journal of Wind Engineering*, 87, 61–79.
- Omenzetter, P., Wilde, K., and Fujino, Y. (2000b). "Suppression of wind-induced instabilities of a long span bridge by a passive deck-flaps control system part II: Numerical simulations." *Journal of Wind Engineering*, 87, 81–91.
- Omenzetter, P., Wilde, K., and Fujino, Y. (2002a). "Study of passive deck-flaps flutter control system on full bridge model 1: Theory." *Journal of Engineering Mechanics*, March, 264–279.
- Omenzetter, P., Wilde, K., and Fujino, Y. (2002b). "Study of passive deck-flaps flutter control system on full bridge model 2: Results." *Journal of Engineering Mechanics*, March, 280–286.
- Ostenfeld, K. H. and Larsen, A. (1992). "Bridge engineering and aerodynamics." *In Aerodynamics of Large Bridges, Proceedings of the First International Symposium on Aerodynamics of Large Bridges*, Copenhagen, Denmark.
- Papageorgiou, C. and Smith, M. C. (2006). "Positive real synthesis using matrix inequalities for mechanical networks: Application." *IEEE Trans. on Control Systems Technology*, 14(3), 423–435.
- Phan, D.-H. and Nguyen, N.-T. (2013). "Flutter and buffeting control of long-span suspension bridge by passive flaps: Experiment and numerical simulation." *International Journal Aeronautical and*

- 728 *Space Sciences*, 14(1).
- 729 Pourzeynali, S. and Datta, T. K. (2005). "Semiactive fuzzy logic control of suspension bridge
730 flutter." *Journal of Structural Engineering, ASCE*, 131, 900–912.
- 731 Scanlan, R. H. (1978). "The action of flexible bridges under wind, I: Flutter theory." *Journal of*
732 *Sound and Vibration*, 60(2), 187–199.
- 733 Scanlan, R. H. and Tomko, J. J. (1971). "Airfoil and bridge deck flutter derivatives." *Journal of*
734 *Engineering Mechanics*, 97(6), 1717–1737.
- 735 Skogestad, S. and Postlethwaite, I. (2006). *Multivariable Feedback Control: Analysis and Design*.
736 2nd Ed. Wiley.
- 737 Smith, M. C. (2002). "Synthesis of mechanical networks: The inerter." *IEEE Trans. Automatic*
738 *Control*, 47(10), 1648–1662.
- 739 Starossek, U. and Aslan, H. (2008). "Passive control of bridge deck flutter using tuned mass dampers
740 and control surfaces." *7th European Conference on Strcutural Dynamics*, Southampton, United
741 Kingdom.
- 742 Theodorsen, T. (1934). "General theory of aerodynamic instability and the mechanisms of flutter."
743 *NACA Report, TR-496*.
- 744 Theodorsen, T. and Garrick, I. E. (1942). "Nonstationary flow about a wing-aileron-tab combination
745 including aerodynamic balance." *NACA Report, TR-736*.
- 746 Wilde, K., Fujino, Y., and Kawakami, T. (1999). "Analytical and experimental study on passive
747 aerodynamic control of flutter of a bridge deck." *Journal of Wind Engineering and Industrial*
748 *Aerodynamics*, 80, 105–119.
- 749 Xiang, H. F. and Ge, Y. J. (2003). "On aerodynamic limit to suspension bridges." *11th International*
750 *Conference on Wind Engineering*, Texas USA.
- 751 Xiaowei, Z., Limebeer, D. J. N., and Graham, M. J. R. (2014). "Modelling and control of a
752 suspended-span bridge section." *19th World Congress, The International Federation of Automatic*
753 *Control*, Cape Town, South Africa.
- 754 Zhao, X., Limebeer, D., and Graham, J. (2011). "Flutter control of long-span suspension bridges."

755 *50th IEEE Conference on Decision and Control and European Control Conference (CDC-ECC),*
756 *Orlando,FL,USA (December).*

List of Tables

1	Physical parameters of the Humber Bridge suspension bridge section with controllable flap	33
2	Aeroelastic limits and robustness indexes for the 3 cases of Deck-Flap configurations, values of stiffness and damping about the flap connections are given per unit span.	34
3	Flutter critical wind speeds and maximum allowable torsional variations (Max. Tor. Variation) at zero wind speed torsional natural frequency for the deck-flap configuration 2 and two variations of the deck-flap configuration 3 (3a,3b), see Fig. 6. Flap controller transfer functions (T.F.) are also included. Parameters are given for a unit span section.	35
4	Flutter critical wind speeds, maximum allowable variations at zero wind speed torsional natural frequency (Max. Tor. Var.) and mechanical network parameters for the first order compensators presented in Table 3. Values are given per unit span.	36
5	Aerodynamic limits and optimized TMD mechanical components when the right TMD mass is 3.5%, Case TMD1, and 7%, Case TMD2, of the deck mass. The left TMD mass is 7% of the deck mass. Values are given for a unit span.	37
6	Optimized mechanical FMD components for the 3 hinge locations cases depicted in Fig. 6. Damping ratios are defined as: $\zeta_{dl} = \frac{C_{dl}}{2\omega_{dl}m_{dl}}$ and $\zeta_{dr} = \frac{C_{dr}}{2\omega_{dr}m_{dr}}$. Values are given for a unit span.	38
7	Aeroelastic performance limits for optimized mechanical FMD components for the 3 hinge locations depicted in Fig. 6.	39

Parameters	Values
b	14.25 m
m	13215 kg/m
I_α	$1.05 \times 10^6 \text{ kgm}^2/\text{m}$
ω_α	1.973 rad/s
ω_h	0.767 rad/s
ρ	1.23 kg/m^3
ρ_f	7850 kg/m^3
d_f	0.025 m
ζ_h	0.01
ζ_α	0.01

TABLE 1. Physical parameters of the Humber Bridge suspension bridge section with controllable flap

Cases	Flutter Speed	Divergence Speed	Rob. Index(γ)	Stiffness $K_{\beta_l} = K_{\beta_t}$	Damping ratio
1	65m/s	72m/s	31.33	$1.05 \times 10^6 \text{ kNm/rad}$ ($\omega_{\beta_l} = \omega_{\beta_t} = 14\omega_\alpha$)	2.11%
2	76m/s	82m/s	90.85	$1.84 \times 10^5 \text{ kNm/rad}$ ($\omega_{\beta_l} = \omega_{\beta_t} = 11.78\omega_\alpha$)	10.1%
3	88m/s	108m/s	4.12	$2.41 \times 10^5 \text{ kNm/rad}$ ($\omega_{\beta_l} = \omega_{\beta_t} = 6.75\omega_\alpha$)	3.52%

TABLE 2. Aeroelastic limits and robustness indexes for the 3 cases of Deck-Flap configurations, values of stiffness and damping about the flap connections are given per unit span.

Cases	Flutter Speed (m/s)	Max. Tor. Variation (%)	Stiffness $K_\beta = K_\gamma$ (kNm/rad)	Damp. Ratio $C_b = C_\gamma$ (%)	T.F. Leading Flap (Nm/(rad/s))	T.F. Trailing Flap (Nm/(rad/s))
2	78	5%	1.97×10^5	2.77	$\frac{1.43 \times 10^6 s + 363000}{11.97s + 45.69}$	$\frac{0.78 \times 10^6 s + 72440}{7.87s + 34.58}$
3a	89	3%	2.48×10^5	0.16	$\frac{762500s + 75}{13.92s + 83.01}$	$\frac{1.27 \times 10^6 s + 120}{33.87s + 301.5}$
3b	86	5%	2.33×10^5	1.34	$\frac{922500s + 90}{16.71s + 81.97}$	$\frac{1.46 \times 10^6 s + 145}{44.41s + 300}$

TABLE 3. Flutter critical wind speeds and maximum allowable torsional variations (Max. Tor. Variation) at zero wind speed torsional natural frequency for the deck-flap configuration 2 and two variations of the deck-flap configuration 3 (3a,3b), see Fig. 6. Flap controller transfer functions (T.F.) are also included. Parameters are given for a unit span section.

Cases	Flutter Speed	Max. Torsion Variation	Leading Flap Network	Trailing Flap Network
2	78m/s	5%	c1=54777.3 Ns/rad c2=0.9 Ns/rad b=9185.8 kgm ²	c1=37584.9 Ns/rad c2=0.398 Ns/rad b=4222.3 kgm ²
3a	89m/s	3%	c1=119632.4 Ns/rad c2=8509.9 Ns/rad b=33571.1 kgm ²	c1=99047 Ns/rad c2=2140.4 Ns/rad b=23029 kgm ²
3b	86m/s	5%	c1=55206.5 Ns/rad c2=1.1 Ns/rad b=11254.3 kgm ²	c1=32864.2 Ns/rad c2=0.48 Ns/rad b=4865.1 kgm ²

TABLE 4. Flutter critical wind speeds, maximum allowable variations at zero wind speed torsional natural frequency (Max. Tor. Var.) and mechanical network parameters for the first order compensators presented in Table 3. Values are given per unit span.

Cases	Flutter Speed	Div. Speed	m_{dl}	K_{dl}	ζ_{dl}	m_{dr}	K_{dr}	ζ_{dr}
<i>TMD1</i>	75 m/s	77 m/s	945 kg	39000 kN/m	19.4%	473 kg	222 kN/m	5.2%
<i>TMD2</i>	78 m/s	78 m/s	945 kg	45900 kN/m	19.4%	945 kg	373 kN/m	15.6%

TABLE 5. Aerodynamic limits and optimized TMD mechanical components when the right TMD mass is 3.5%, Case TMD1, and 7%, Case TMD2, of the deck mass. The left TMD mass is 7% of the deck mass. Values are given for a unit span.

Cases	m_{dl} (kg)	ζ_{dl} %	K_{dl} (kN/m)	m_{dr} (kg)	ζ_{dr} %	K_{dr} (kN/m)	T.F. Leading Flap Controller (Nm/(rad/s))	T.F. Trailing Flap Controller (Nm/(rad/s))
1	945	19.2	141300	828	4.8	16510	$\frac{-7.35 \times 10^6 s - 1620}{95.68s + 147.8}$	$\frac{-1.89 \times 10^6 s - 1.73 \times 10^6}{18.18s + 68.91}$
2	914.9	11.1	169280	803.7	8.3	28280	$\frac{-1.03 \times 10^7 s - 1460}{86.21s + 233.3}$	$\frac{-8.172 \times 10^6 s - 1245}{70.73s + 208.3}$
3	936.6	7.6	110740	267.2	9.5	43390	$\frac{-883000s - 80}{101.5s + 32.26}$	$\frac{-285000s - 30}{10.36s + 52.62}$

TABLE 6. Optimized mechanical FMD components for the 3 hinge locations cases depicted in Fig. 6. Damping ratios are defined as: $\zeta_{dl} = \frac{C_{dl}}{2\omega_{dl}m_{dl}}$ and $\zeta_{dr} = \frac{C_{dr}}{2\omega_{dr}m_{dr}}$. Values are given for a unit span.

Cases	Flutter Speed	Div. Speed	Rob. Index	Max. Tor. Variation
1	110 m/s	81 m/s	2.58	2 ‰
2	117 m/s	86 m/s	3.62	3 ‰
3	93 m/s	104 m/s	2.7	5 ‰

TABLE 7. Aeroelastic performance limits for optimized mechanical FMD components for the 3 hinge locations depicted in Fig. 6.

List of Figures

1	Idealized cross section of a long-span suspension bridge with a controllable leading-trailing-edge flaps. a) The flaps are adjacent to the bridge deck b) flaps detached from the deck. The wind speed is denoted by U , the leading-edge flap angle is denoted by β_l and the trailing-edge flap angle by β_t	42
2	Mechanical networks for flutter suppression proposed by a) (Omenzetter et al. 2000a), b) (Wilde et al. 1999).	43
3	(a) Kinematic model of the bridge deck (Graham et al. 2011). The wind velocity U is assumed positive to the right, the heave h and lift force L are assumed to be positive downwards, moments M are positive clockwise, as are the pitch and trailing-edge flap angles α and β_t respectively. The leading-edge flap angle β_l is positive anti-clockwise. The deck chord (including the flaps) is $2b$. The leading- and trailing-edge flap chords are $(1 + c_l)b$ and $(1 - c_t)b$ respectively; note that c_l is a negative quantity. (b) Bridge deck-flap system notation.	44
4	Block diagram of the open-loop aerodynamic system of the four DOF sectional model.	45
5	Block diagram of the aeroelastic control system.	46
6	Three configurations of flap hinge location.	47
7	Root-loci of the uncontrolled Humber Bridge sectional model. The wind speed is swept from 0m/s to 85m/s, with the low-speed ends of the root loci marked with 'red' hexagons and the high-speed ends with 'blue' hexagons. The pitch mode goes unstable at approximately 65m/s and the torsional divergence mode goes unstable at approximately 72m/s.	48

802	8	Root-loci for the deck-flap assembly connected with springs and dampers for the	
803		three hinge positions. The wind speed is swept from 0 m/s to 90 m/s, with the	
804		low-speed end of the root loci marked with (magenta) hexagons and the high-speed	
805		ends marked with (green) crosses. The onset of aeroelastic instabilities for these	
806		cases are summarized in Table 2.	49
807	9	a) Root loci of the deck-flap system corresponding to case 2 for 1% variation in the	
808		zero wind speed torsional natural frequency. b) Root loci of the deck-flap system	
809		corresponding to case 3 for 2% variation in the zero wind speed torsional natural	
810		frequency.	50
811	10	A-free-body diagram of a one-port (two-terminal) mechanical element or network	
812		with force velocity pair (F, v) where $v = U_2 - U_1$	51
813	11	Realization of a first-order mechanical compensator.	52
814	12	Transient response of deck pitch and flap rotations for the configuration of passive	
815		network case 3b. Initial condition is a 2deg pitch of the deck and considered wind	
816		speeds are 75m/s and 85m/s.	53
817	13	The TMD control system consists of two suspended masses symmetrically placed	
818		about the section's elastic center. The flaps are assumed rigidly attached to the deck	
819		by using high stiffness values at the deck-flap connections, K_{β_l} and K_{β_r}	54
820	14	(a) Root Loci for different added mass ratios ranging from $\mu = 0.01$ to $\mu = 0.3$. The	
821		masses are considered fixed to the deck. (b) Corresponding critical wind-speeds	
822		and instability modes.	55
823	15	(a) Transient response of the deck pitch (b) transient response of the TMD mass	
824		movement for the 2 cases presented in Table 5	56
825	16	Conceptual mechanical configuration of the Flap Mass Damper (FMD).	57
826	17	Root Loci of case 3b of Table 3 and case 3 of Table 7. The wind velocities are	
827		swept from 0 to 100m/s.	58

828	18	Transient response of deck heave, deck pitch and flap rotations for cases 3b of Table	
829		3, case 3 of Table 7 and case TMD2 of Table 5.	59
830	19	Vertical mass movement of the mass dampers for cases TMD2 from Table 5 and	
831		Case 3 from Table 7 and for wind speeds (a) 76m/s, both TMD and FMD stable,	
832		(b) 90m/s, FMD stable and TMD unstable.	60
833	20	Effectiveness of TMD (a) and FMD (b) against tuning frequency	61

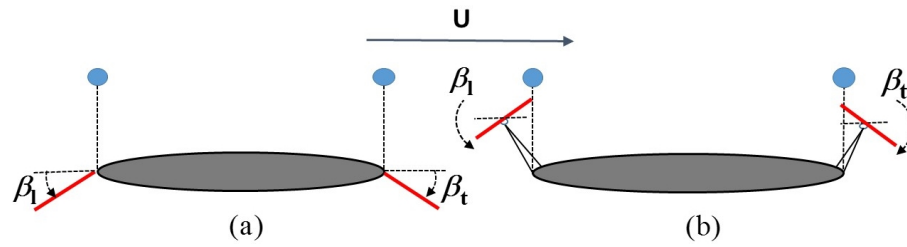


Fig. 1. Idealized cross section of a long-span suspension bridge with a controllable leading-trailing-edge flaps. a) The flaps are adjacent to the bridge deck b) flaps detached from the deck. The wind speed is denoted by U , the leading-edge flap angle is denoted by β_l and the trailing-edge flap angle by β_t .

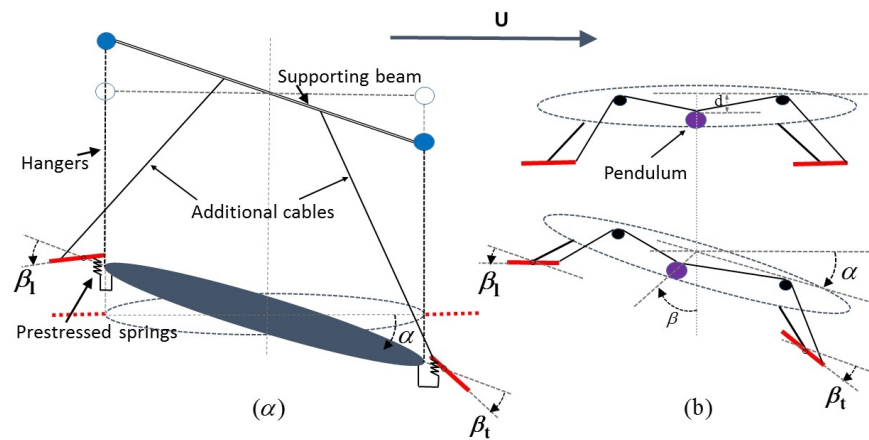


Fig. 2. Mechanical networks for flutter suppression proposed by a) (Omenzetter et al. 2000a), b) (Wilde et al. 1999).

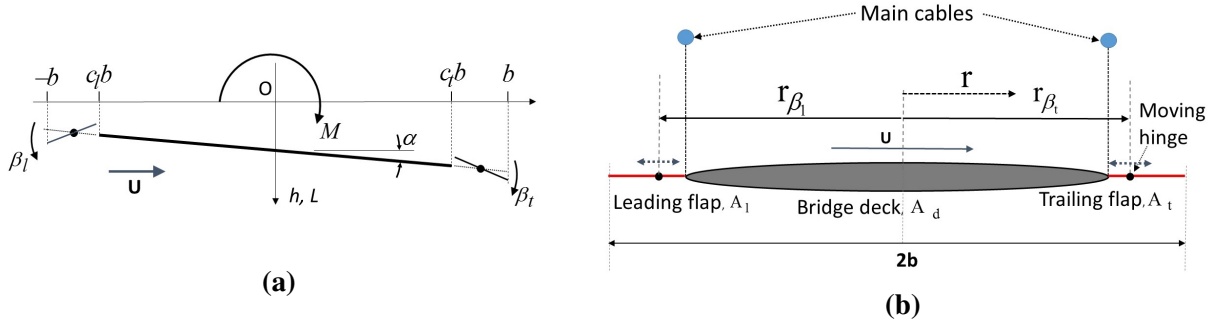


Fig. 3. (a) Kinematic model of the bridge deck (Graham et al. 2011). The wind velocity U is assumed positive to the right, the heave h and lift force L are assumed to be positive downwards, moments M are positive clockwise, as are the pitch and trailing-edge flap angles α and β_t respectively. The leading-edge flap angle β_l is positive anti-clockwise. The deck chord (including the flaps) is $2b$. The leading- and trailing-edge flap chords are $(1 + c_l)b$ and $(1 - c_t)b$ respectively; note that c_l is a negative quantity. (b) Bridge deck-flap system notation.

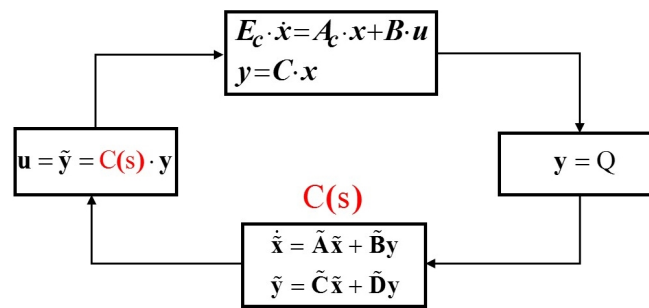


Fig. 4. Block diagram of the open-loop aerodynamic system of the four DOF sectional model.

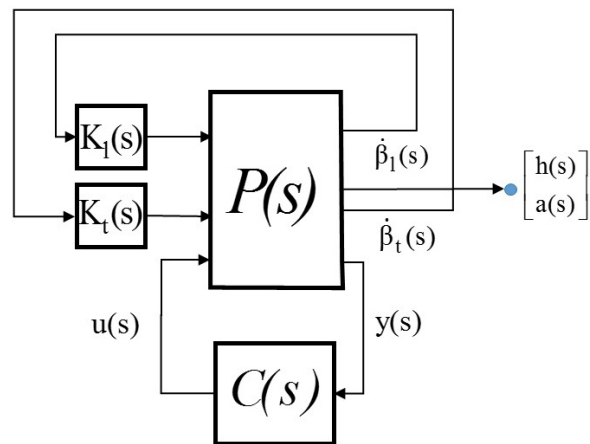


Fig. 5. Block diagram of the aeroelastic control system.

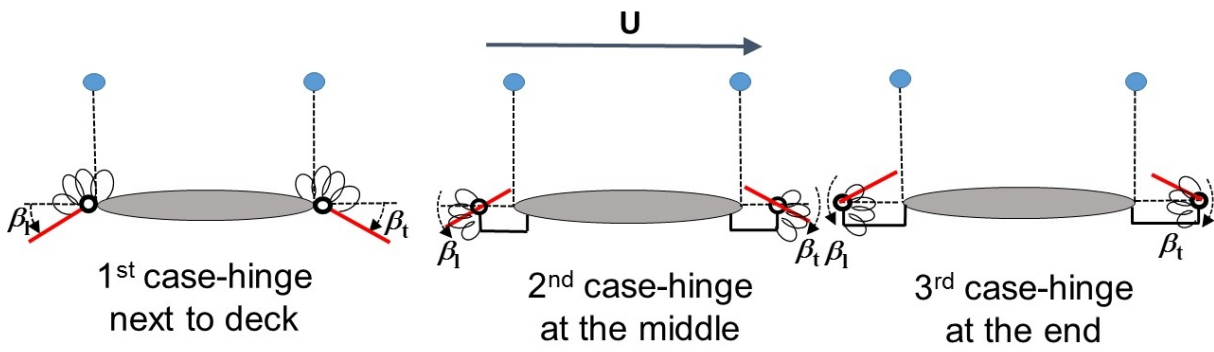


Fig. 6. Three configurations of flap hinge location.

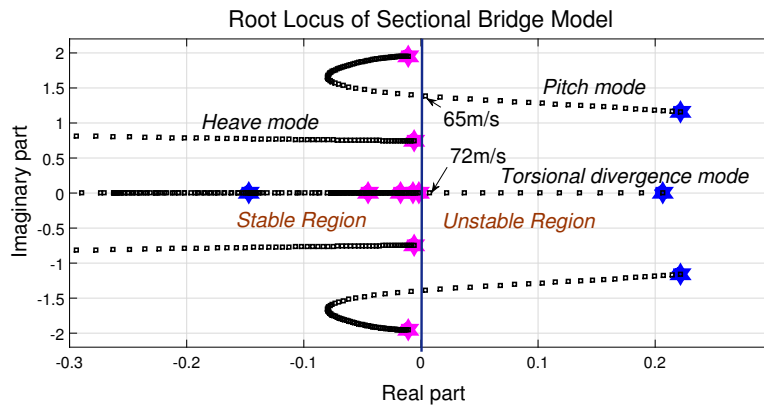


Fig. 7. Root-loci of the uncontrolled Humber Bridge sectional model. The wind speed is swept from 0m/s to 85m/s, with the low-speed ends of the root loci marked with 'red' hexagons and the high-speed ends with 'blue' hexagons. The pitch mode goes unstable at approximately 65m/s and the torsional divergence mode goes unstable at approximately 72m/s.

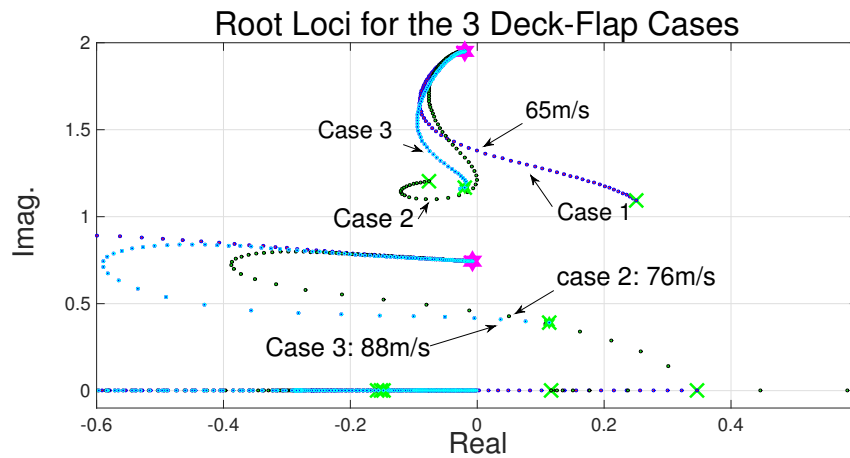


Fig. 8. Root-loci for the deck-flap assembly connected with springs and dampers for the three hinge positions. The wind speed is swept from 0 m/s to 90 m/s, with the low-speed end of the root loci marked with (magenta) hexagons and the high-speed ends marked with (green) crosses. The onset of aeroelastic instabilities for these cases are summarized in Table 2.

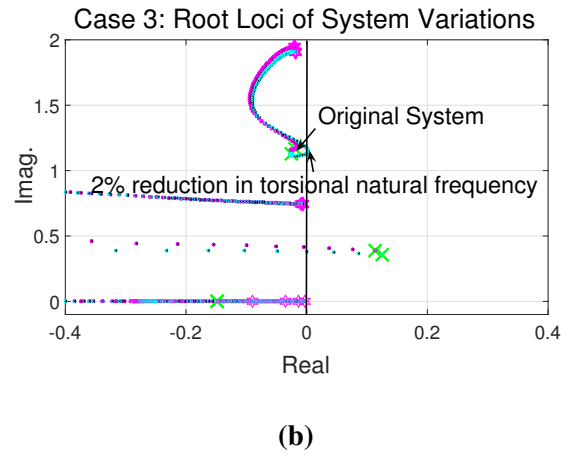
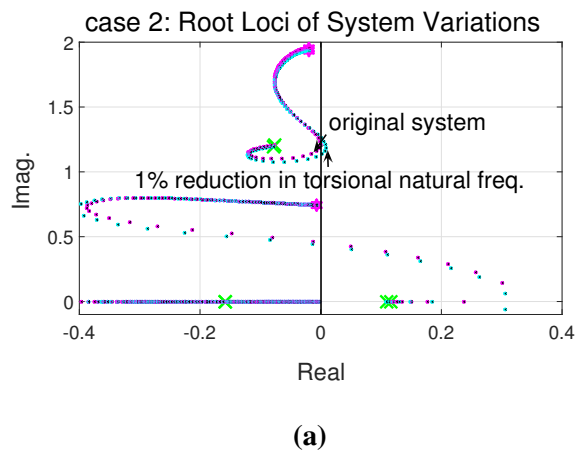


Fig. 9. a) Root loci of the deck-flap system corresponding to case 2 for 1% variation in the zero wind speed torsional natural frequency. b) Root loci of the deck-flap system corresponding to case 3 for 2% variation in the zero wind speed torsional natural frequency.

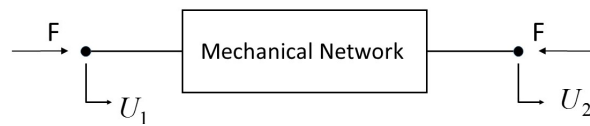


Fig. 10. A-free-body diagram of a one-port (two-terminal) mechanical element or network with force velocity pair (F, v) where $v = U_2 - U_1$.

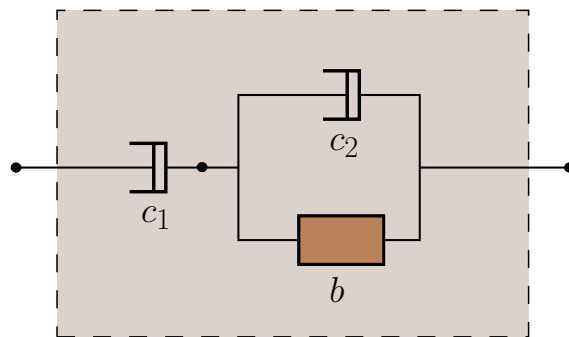


Fig. 11. Realization of a first-order mechanical compensator.

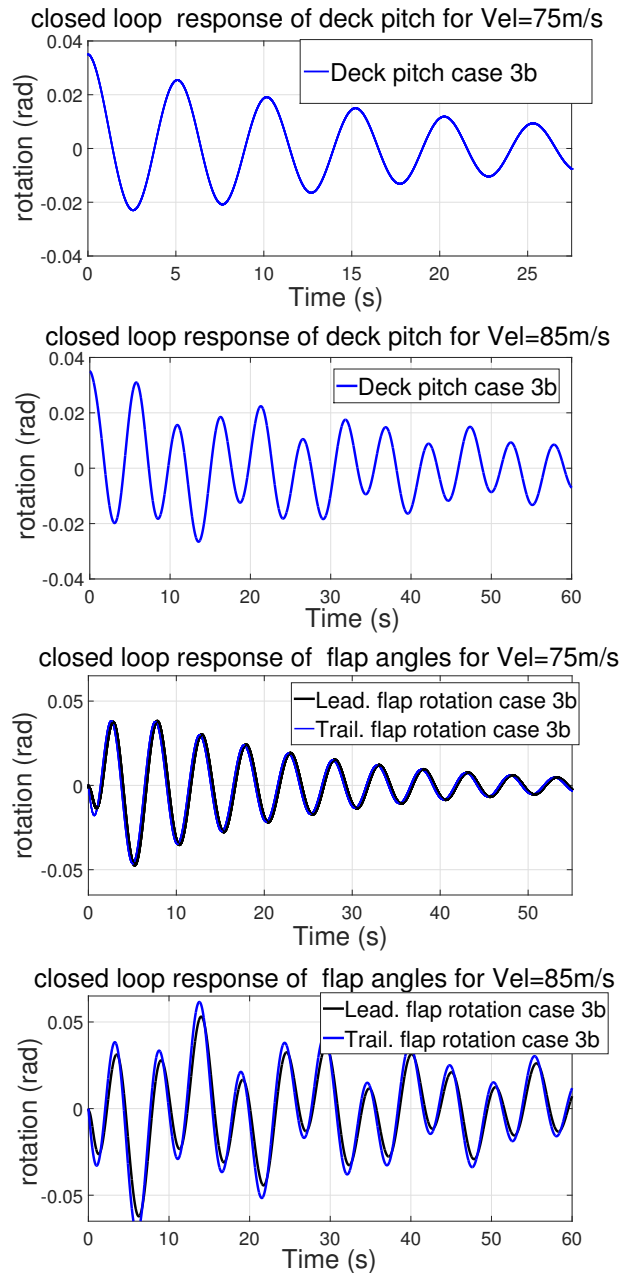


Fig. 12. Transient response of deck pitch and flap rotations for the configuration of passive network case 3b. Initial condition is a 2deg pitch of the deck and considered wind speeds are 75m/s and 85m/s.

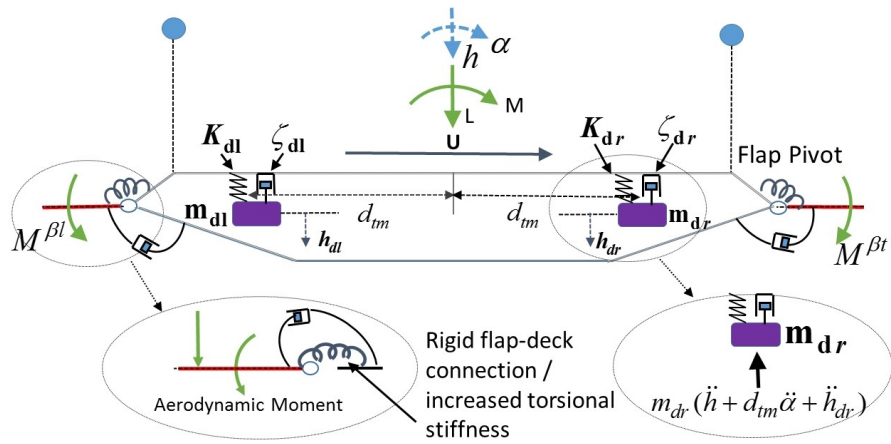


Fig. 13. The TMD control system consists of two suspended masses symmetrically placed about the section's elastic center. The flaps are assumed rigidly attached to the deck by using high stiffness values at the deck-flap connections, K_{β_l} and K_{β_t} .

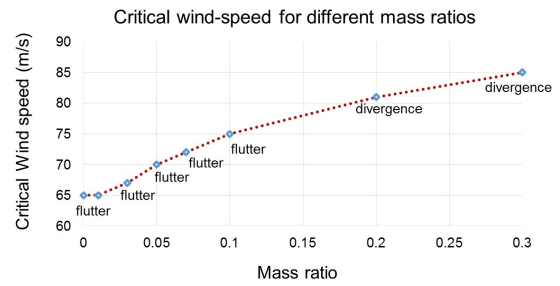
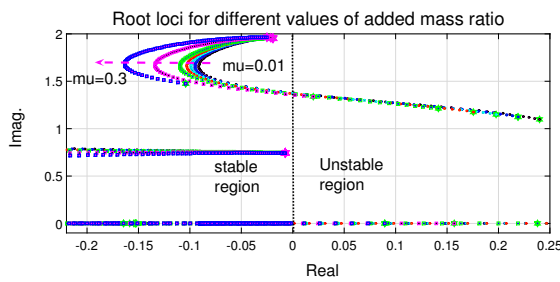


Fig. 14. (a) Root Loci for different added mass ratios ranging from $\mu = 0.01$ to $\mu = 0.3$. The masses are considered fixed to the deck. (b) Corresponding critical wind-speeds and instability modes.

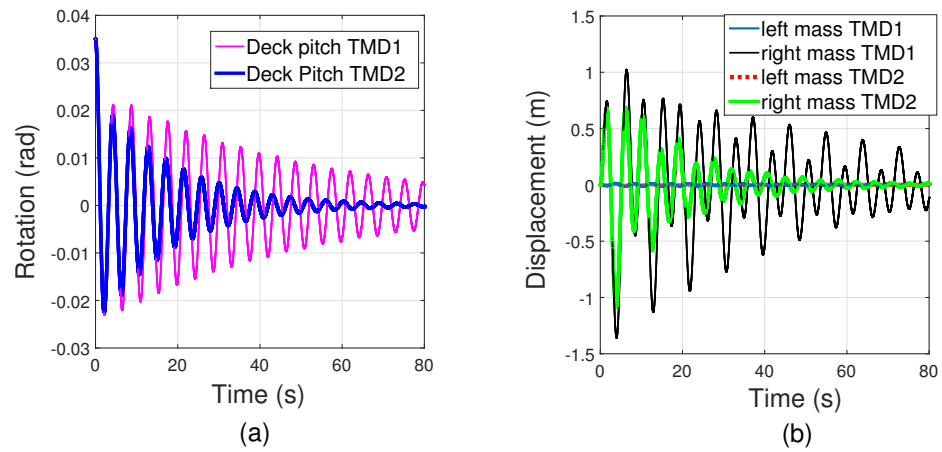


Fig. 15. (a) Transient response of the deck pitch (b) transient response of the TMD mass movement for the 2 cases presented in Table 5



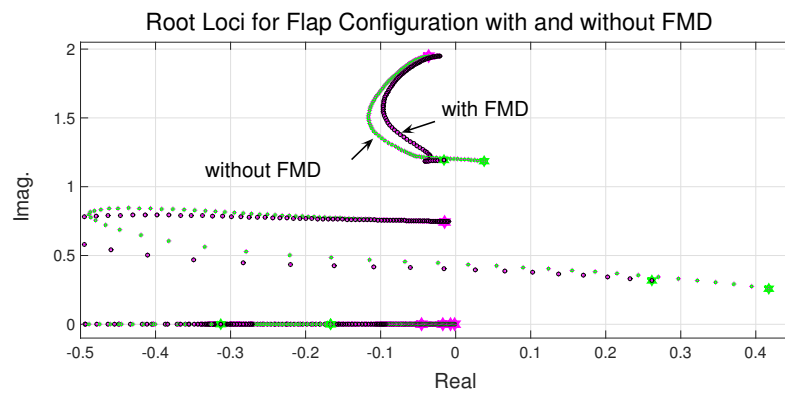


Fig. 17. Root Loci of case 3b of Table 3 and case 3 of Table 7. The wind velocities are swept from 0 to 100m/s.

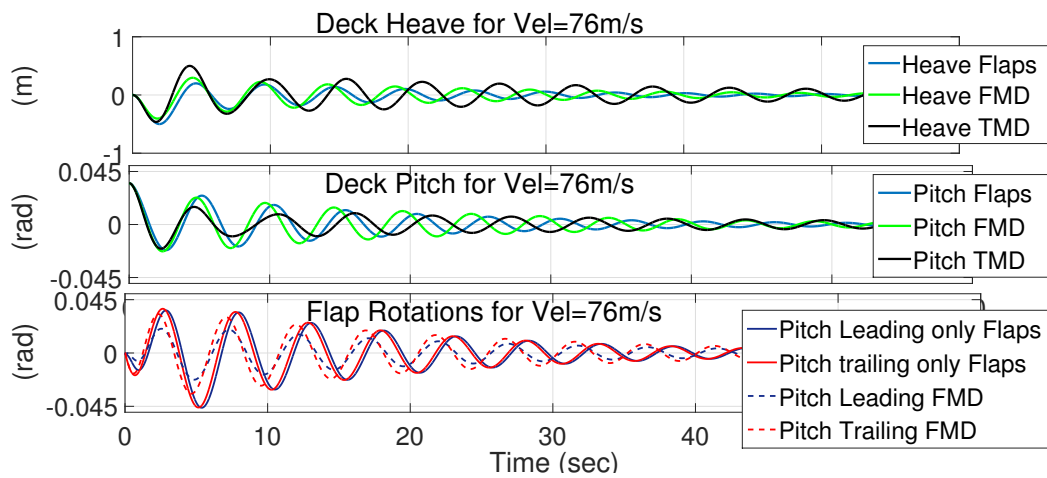


Fig. 18. Transient response of deck heave, deck pitch and flap rotations for cases 3b of Table 3, case 3 of Table 7 and case TMD2 of Table 5.

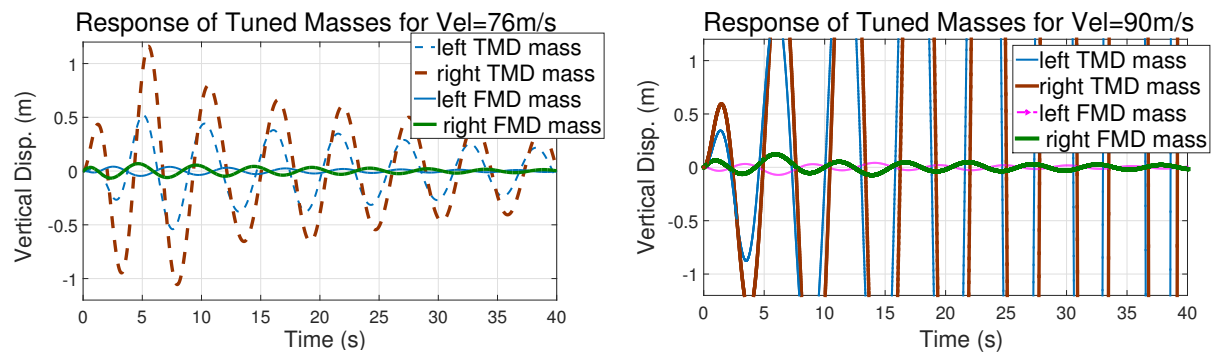


Fig. 19. Vertical mass movement of the mass dampers for cases TMD2 from Table 5 and Case 3 from Table 7 and for wind speeds (a) 76m/s, both TMD and FMD stable, (b) 90m/s, FMD stable and TMD unstable.

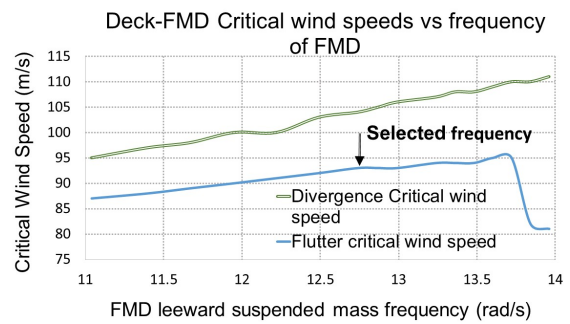
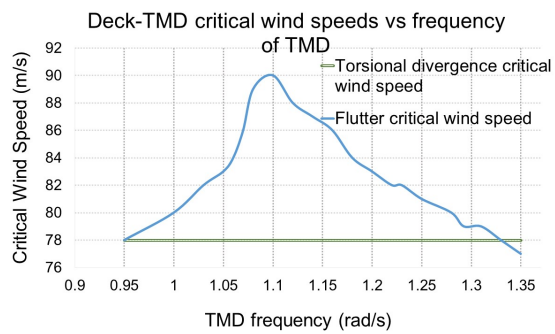


Fig. 20. Effectiveness of TMD (a) and FMD (b) against tuning frequency